

# Technical Report

## Automatic Contour Extraction from 2D Neuron Images

J. J. G. Leandro<sup>a,\*</sup>, R. M. Cesar-Jr<sup>a</sup>, L. da F. Costa<sup>b</sup>

<sup>a</sup>*Institute of Mathematics and Statistics - USP, Department of Computer Science  
Rua do Matão, 1010 - São Paulo - SP, 05508-900 Brazil*

<sup>b</sup>*Instituto de Física de São Carlos - USP, Department of Physics and Informatics  
Av. Trabalhador São-carlense, 400 - São Carlos - SP, 13560-970 Brazil*

---

### Abstract

This work describes a novel methodology for automatic contour extraction from 2D images of 3D neurons (e.g. camera lucida images and other types of 2D microscopy). Most contour-based shape analysis methods can not be used to characterize such cells because of overlaps between neuronal processes. The proposed framework is specifically aimed at the problem of contour following even in presence of multiple overlaps. First, the input image is preprocessed in order to obtain an 8-connected skeleton with one-pixel-wide branches, as well as a set of *critical regions* (i.e., bifurcations and crossings). Next, for each subtree, the tracking stage iteratively labels all valid pixel of *branches*, up to a *critical region*, where it determines the suitable direction to proceed. Finally, the labeled *skeleton segments* are followed in order to yield the *parametric contour* of the neuronal shape under analysis. The reported system was successfully tested with respect to several images and the results from a set of three neuron images are presented here, each pertaining to a different class, i.e. alpha, delta and epsilon ganglion cells, containing a total of 34 crossings. The algorithms successfully got across all these overlaps. The method has also been found to exhibit robustness even for images with close parallel segments. The proposed method is robust and may be implemented in an efficient manner. The introduction of this approach should pave the way for more systematic application of contour-based shape analysis methods in neuronal morphology.

*Key words:* Contour extraction, branching structures, neuron, shape analysis, image processing, neuronal morphology, pattern recognition

---

\* Corresponding author.

*Email addresses:* jleandro@vision.ime.usp.br (J. J. G. Leandro), cesar@vision.ime.usp.br (R. M. Cesar-Jr), luciano@ifsc.usp.br (L. da F. Costa).

## 1 Introduction

Neurons can be understood as cells specialized in interconnections, which are implemented through synapses extending from axonal to dendritic arborizations. Though the connectivity of mature neuronal systems may seem to be stable, it is actually subjected to continuing re-organizations influenced by stimuli presentation and biological changes. The number of connections which a neuron may receive is to a large extent defined by the shape of its dendritic tree, which serves as a target for growing axons. As a consequence, the full understanding of the functionality of neuronal circuits requires the proper characterization of the neuronal morphology (e.g. [7, 9, 20]). Among the several approaches based on the characterization of the geometry and connectivity of neuronal cells [3, 9, 14, 19, 20], a particularly important and broad set of shape analysis algorithms relies on a parametric representation of the neuronal shape [8], i.e. in the form  $c(t) = (x(t), y(t))$ .<sup>1</sup> The proper contour extraction of 2D neuron images yields parametric signals, from which features can be calculated and used to characterize differences between neuronal shapes. Despite the availability of algorithms to extract parametric contours from digital images, they can not be applied directly in neuroscience because of the intense overlap (crossings) which is frequently observed among the neuronal processes. In order to better appreciate this limitation, please refer to Fig. 1.

Often, the 3D neurons are projected into the 2D space (e.g. camera lucida and several types of 2D microscopy), so that the contour of the cells can, in principle, be represented as 1D parametric curves [12] (Fig. 1(a)). Important information, such as the normal and/or tangent orientation fields along such contours, as well as the arc length of each segment, can then be obtained, allowing the estimation of important geometrical properties such as the contour curvature and wavelets (e.g. [5, 9]), which are known to provide particularly valuable information about the shape of the neuron, including its bending and concavity. Another possible application of contours in neuroscience is as a means to automatically obtain neuronal dendrograms [6]. However, such an approach is often complicated by the presence of crossings between the neuronal processes in the 2D image, implying some regions of the cell to become inaccessible for traditional contour extraction algorithms (see Fig.1(b)). Henceforth, we refer to such inaccessible contour portions as the *innermost regions* of the shape. In brief, most contour following algorithms work as follows. Firstly, the algorithm detects an initial contour pixel. Then, the algorithm searches the next contour pixel, by probing the current contour pixel vicinity. The algorithm travels around the whole object, until revisiting the first pixel, once the task has been completed. Further details can be found in the full description of such methods in [8].

In contour following algorithms, it is usually impossible to traverse the innermost

---

<sup>1</sup> For instance, a circle may be represented as  $c(t) = (x(t), y(t)) = (\cos(t), \sin(t))$

regions delimited by crossings (due to the 3D to 2D projection). Consequently, only the outer contour of the cell is represented, thus missing the innermost structures. This fact is illustrated in Fig. 1(b), where the light gray shaded innermost regions represent areas inaccessible to traditional contour following algorithms, thus yielding just the red curve as the respective contour.

It should be observed that, in principle, 3D imaging is naturally better than 2D imaging because it contains more information about the acquired structure. However, 3D imaging intrinsically demands additional computational resources, especially for the enhancement and interpretation of the structures. In addition, in cases where the original neurons are mostly planar, such as the ganglion cells in the retina, the 3D capture often contributes little to the separation between thin crossing segments, which are mostly contained within a narrow range of  $z$ -coordinates. Another reason why 2D imaging remains valuable in neuroscience concerns the fact that not all types of microscopy can be performed in 3D. Finally, many 2D neuron imaging systems and images are already available (e.g. camera lucida images from previous experiments and published literature), so that research using such images would also benefit from the introduction of the methodology proposed in the present paper.

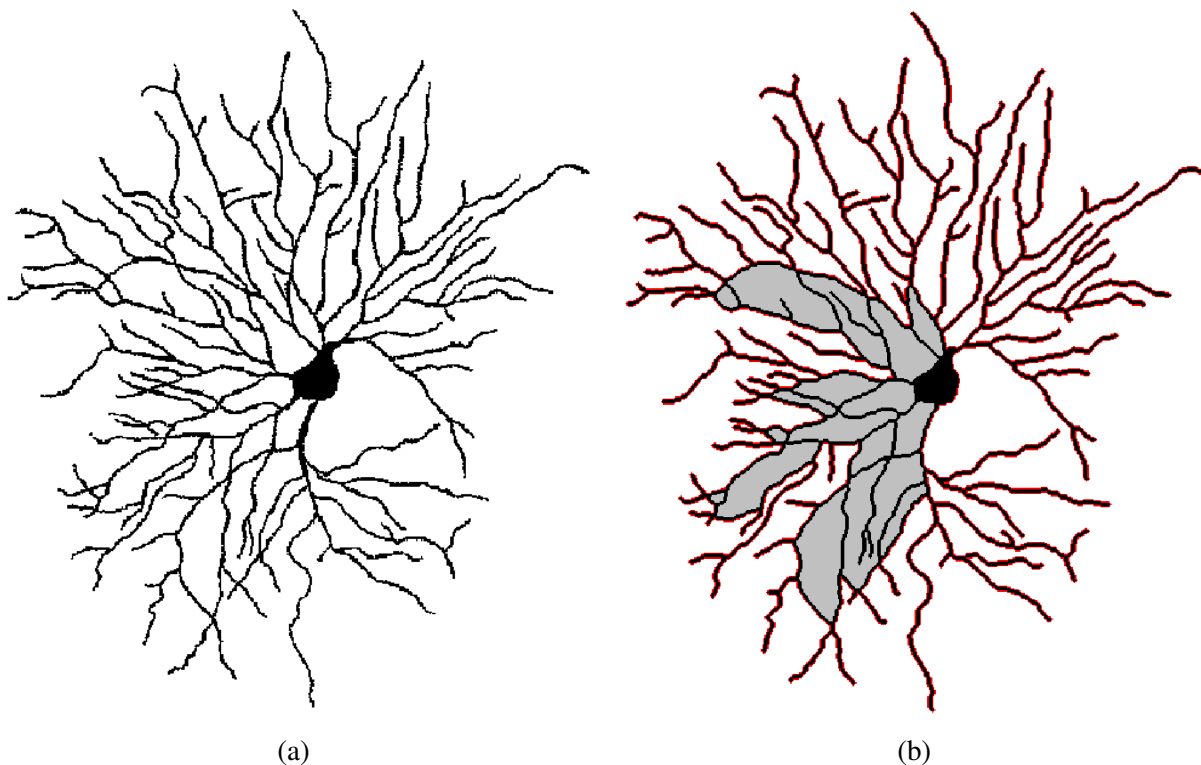


Fig. 1. (a) Example of 2D neuron image considered in this work. (b) Neuron image (black) and respective contour (red) as provided by a traditional contour following algorithm. The light gray shaded areas represent the innermost regions that remain inaccessible for such algorithms.

Despite the importance of the problem of contour extraction from  $2D$  neuron images, we were not able to find any related approaches in the literature. To the best of our knowledge, the only similar work in the literature was described in [21, 22], which presents a semi-automatic method to separate veins and arteries in the vascular trees of fundus images. In order to solve such a problem, it is necessary to label the vessels, which are also branching structures. Firstly, a skeleton image is obtained from the vessel trees. The skeleton is then represented as a vascular graph named  $G$ , which comprises all the information regarding the connectivity among critical regions and branches segments. Subsequently, that method propagates the labels manually assigned to other vessels throughout the vascular graph  $G$ . In this case, it is well-known that crossings only take place between a vein and an artery, thus such a priori knowledge on the vessels structure is used to simplify the approach, determining that opposite branches segments in a crossing should be necessarily equally labeled. Such assumptions make this approach specific to the vein/artery tracing problem. Alternatively, neighbouring branches segments in a crossing should be labeled with distinct tags. Although there are some similarities between the approaches reported in [21, 22] and in the current article (mainly concerning the use of skeletons and case analysis of bifurcations and crossings), the latter methodology adopts a different and potentially more general approach. Since the aforementioned system has been specially designed for vascular trees, the number of labels available to be assigned is bounded to two: veins and arteries. Conversely, our algorithms yield assignments of a distinct label for each existing branch and also a distinct label for each dendritic tree, regardless of the number of existing dendritic trees in the neuron. Also, by segmenting each branch within the image, our method allows the branches to be counted as well as the lengths of the segments to be measured. In contrast to the Rothaus' system, ours solely carries out local assessment of the image topology in a sequential-like fashion, without graph representations, thus avoiding the backtracking step. Furthermore, our system provides the parametric contour of the whole structure, being thus possible to extract several geometrical features to be fed to a classifier.

Also, the results reported in our work can also be useful for the unsolved  $3D$  cases by confocal microscopy. In addition, there are more important aspects regarding the importance and applicability of our contribution, and these are as follows. First, there are dozens of other microscopic techniques which cannot yield  $3D$ , but only  $2D$  images, necessarily implying tangling of neuronal branches which can be treated by our method. Such microscopy techniques are often required instead of confocal microscopy because they can reveal specific properties of the analyzed tissues and structures which cannot be imaged by confocal methodology.

Moreover, as already mentioned, the proposed methodology is quite general and may be applied to other branching structures.

The rationale of the present work is to deal with neuronal overlaps by incorporating several criteria such as the use of similarities along the tangent orientation as a

means to identify the proper continuation of the neuronal processes at crossing-points. The proposed methodology is composed by the subsequent application of the following three algorithms:

- (1) Preprocessing
- (2) *Branches Tracking Algorithm (BTA)*
- (3) *Branching Structures Contour Extraction Algorithm (BSCEA)*

In short, the *BTA* is an algorithm aimed at the segmentation of each distinct branch within a  $2D$  neuron image other than the soma and intercepting regions. The *BSCEA* is an algorithm intended to the extraction of the parametric contour from a  $2D$  neuron image, based on the *BTA*.

For clarity's sake, this paper is presented in increasing levels of detail, hence developing as follows. Section 2 contains an overview of the proposed framework, which is further detailed in Section 3. Experimental results considering real neuronal cells are presented in Section 4. The paper concludes in Section 5, by identifying the main contributions, as well as possibilities for future works. Low level descriptions has been left to the Appendices A.2 and A.1.

## 2 Preamble

Usually, an optical acquisition device yields an image as output, corresponding to a summary and incomplete representation of the information originally present in the original object [4]. As a result, images are normally devoid of some information, such as related to depth, a problem arising from the supression of the third dimension in the  $3D$  original object as implied by its object projection onto the  $2D$  plane. In the context of complex shape images, like neurons, depth information is of extreme importance to properly discern the structures in the image. The current work approaches this problem, more specifically the extraction of contours of neuronal cells imaged onto  $2D$  frames. In particular, the  $2D$  neuron images used herein have been obtained through a camera lucida device.

### 2.1 Terminology

Initially, our approach considered the existence of only two types of structures among branches, namely bifurcations and crossings. However the number of adjacent segments at each critical region proved not to be enough to properly classify them, leading to misclassifications. Only through the incorporation of additional information, namely the identification of several geometrical features along the neuronal shape, it has been possible to achieve correct classification of the critical re-

Table 1  
Summary of concepts.

TERM		DESCRIPTION
Points		
seed	primary	origin of a segment stemming from the soma
	secondary	origin of a segment stemming from a critical region
termination		end point of a branch
Lines		
segment		line of pixels delimited by other structures
inward segment		incoming segment at a critical region
outward segment		outgoing segment from a critical region
branch		string of segments
Critical Regions ( <i>CR</i> )		
bifurcation		cluster of pixels where an inward segment splits into two; one of which in other direction
crossing		cluster of pixels where an inward segment splits into three; two of which in other direction
superposition		cluster of bifurcations where an inward segment splits into three; two of which in other direction
Collections		
dendritic arbour		collection of branches growing out of soma
periphery		collection of dendritic arbours (excluding soma)
skeleton		one-pixel wide skeleton from the periphery

gions. The neuronal shape can be described as the union of its constituent parts, i.e. soma, dendrites or dendritic arbours and axon. In order to elaborate on the explanation of our methods, we extend such a terminology. Notice that it does not refer to additional functional parts in neurons, but rather to morphological building blocks which compose those functional parts in their respective  $2D$  images. As a matter of fact, some structures such as crossings and superpositions do not even occur in a real  $3D$  neuron, being just an immediate consequence of the projection from the  $3D$  space onto the plane or their close proximity even in  $3D$  spaces. Hence, the arbours present in  $2D$  skeletons obtained from neuron images are subdivided into their morphological constituent parts as follows (see Fig. 2 and Tab. 1):

- *Points*
- *Lines*
- *Critical Regions*
- *Collections*

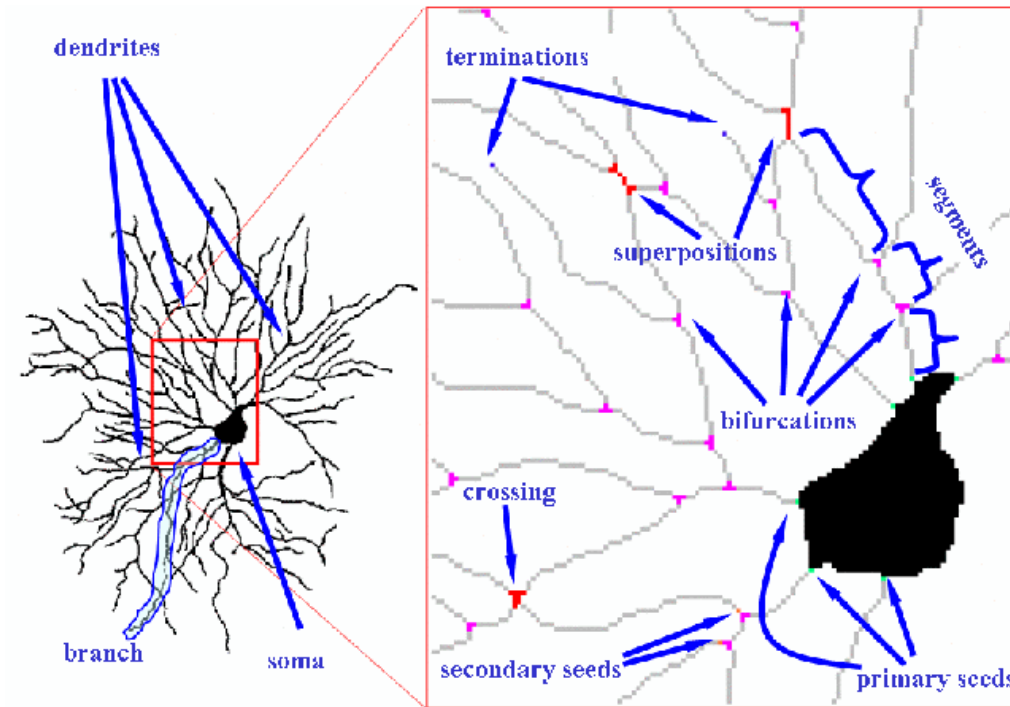


Fig. 2. Extended terminology adopted in this work: dendrites, soma, branches, segments, seeds, terminations and critical regions.

The aforementioned categories of structures encompass the typical structures which usually appear in  $2D$  neuron images. Such structures must be distinguished so as to provide additional information about the original neuronal shape, therefore allowing more general and effective performance.

The category *Points* comprises three classes of extremity points: primary seeds, secondary seeds and terminations. Each extremity point is classified regarding its location, i.e. a *primary seed* corresponds to a junction point between a dendritic tree and the soma, while a *secondary seed* refers to a junction point between a critical region and a dendritic subtree. Basically, the difference between a primary seed and a secondary seed is that a primary seed is necessarily adjacent to the soma, while a secondary seed is not. *Terminations* are end points of branches. The reason for distinguishing between points is that the tracking starts from the primary seeds and finishes at terminations, occasionally repeating itself in a recursive-like fashion from secondary seeds.

The category *Lines* encompasses two cases: segments and branches. Each line is classified with respect to its extremity points, i.e. a segment may grow out from either a primary or a secondary seed, but does not necessarily end at a termination. *Segments* are lines of pixels delimited by a pair of minor structures, for instance a seed and a critical region, or two critical regions, or a critical region and a termination. Conversely, a branch may stem from either a primary or a secondary seed, ending necessarily at a termination. It follows from such a definition that a *branch*

is a ramification made up of a string of segments, growing out of a seed up to a termination, as shown in Fig.2. In addition, segments may be further subclassified depending on their relationship to an adjacent critical region. By analyzing a neuron shape from inside out, that is, from the soma towards its terminations, an incoming adjacent segment to a critical region is said an *inward segment*, while an outgoing adjacent segment to a critical region is said an *outward segment*. The reason for distinguishing between lines is the need to recognize the constituent parts (segments) of branches every time the tracking algorithm reaches a critical region. Adjacent segments which present tangent similarity should be regarded as part of the same branch. Segments and branches play different roles in the tracking algorithm, thus deserving distinct names.

*Critical Regions* are clusters of pixels where branches meet each other. This category includes three classes of regions: bifurcations, crossings and superpositions. Each Critical Region is classified by considering its shape, the number of segments adjacent to it and their mutual orientation relationship, as well as the proximity relationship between the current critical region and other regions nearby. On a *bifurcation*, an inward segment often separates into two outward segments with different orientations, as depicted in Fig.4-(a-b). Occasionally, bifurcations may occur very close one another. Viewing such regions from a larger scale would suggest just one critical region, where an inward segment splits into three outward segments, as shown in Fig.4-(c-d). Similarly, on a *superposition*, an inward segment splits into three outward segments, two of them in normally distinct and opposite orientations, as can be seen in Fig. 4-(e). If superpositions are not considered, they could be locally misunderstood as two very close bifurcations attached by a tiny segment. Finally, a *Crossing Region* is a cluster of pixels where an inward segment splits into three outward segments, two of them in quite distinct and necessarily opposite orientations, as shown in Fig.4-(f).

Though all critical regions share the property of being formed by pixels with neighborhood greater than two, their shape structure are quite different. The reason for distinguishing between critical regions is to assure that both the tracking and the contour extraction algorithms behave as expected whenever such structures are found. The algorithms undergo different processings for each kind of critical region.

At this point, it is worth emphasizing the difference between a crossing and a superposition: although both share the property of having an inward segment splitting into three outward segments, their shapes are slightly different. Notice that a crossing appears as just a cluster of pixels, while a superposition is apparently made up of two clusters of pixels (bifurcations) attached by a short line. In spite of the fact that both structures have been originated from overlapping processes, the angle of inclination between these processes plays a central role, in that the steeper the slope between them, the greater the chance of obtaining a crossing, while the smoother the slope between them, the greater the chance of obtaining a superposition, as



illustrated in Figure 3.

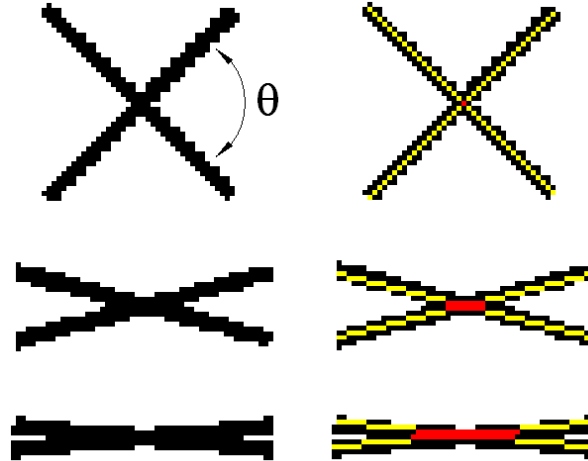


Fig. 3. The dependence between the angle  $\theta$  of inclination between intercepting branches (yellow) and the shape of the respective critical region (red). Observe that as  $\theta$  decreases, more elongated the critical region becomes.

The category *Collections* simply represents groups of the aforedefined objects. A *Dendritic Arbour* is a collection of branches having roots in the soma. Hencerforth the collection of Dendritic Arbours, that is, the neuron without the soma, is simply referred as the *Periphery*. These concepts are summarized in the Table. 1.

## 2.2 System overview

Briefly, the proposed approach for the parametric contour extraction of branching structures involves the following three steps:

- **Input Preprocessing Algorithm.** In summary, this algorithm is aimed at preprocessing the input  $2D$  image, unfolding it into additional images containing its required structural building blocks for the subsequent steps. The input image is preprocessed by means of mathematical morphology operations [10, 24], yielding its separate components, namely:
  - periphery skeleton image, henceforth referred to as skeleton
  - critical regions image
  - terminations image
  - soma image
  - queue of primary seeds
- **Branch Tracking Algorithm.** The **BTA** has two main goals: to label each branch and to classify each critical region. It is applied for every primary seed present in the queue. The labelling procedure starts at the segment adjacent to the primary seed. After reaching a critical region, the current segment will have been entirely labeled, so a decision concerning the next segment to continue with the tracking

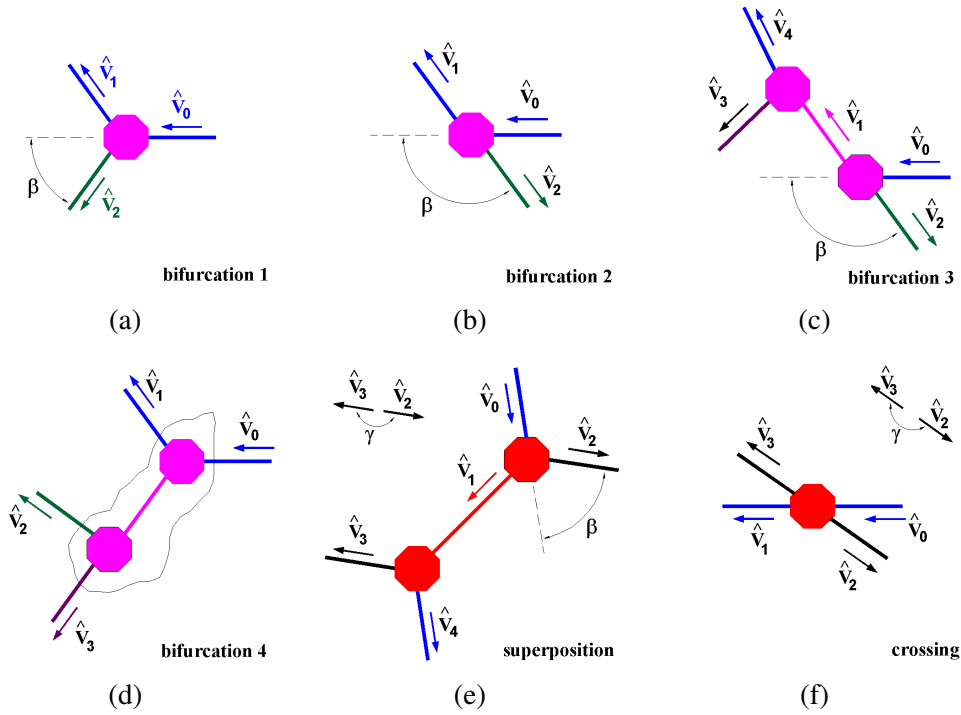


Fig. 4. The critical regions classification rules take into account the angle  $\beta$  between the inwards direction vector -  $\hat{v}_0$  - and the outwards direction vector -  $\hat{v}_2$ , the angle  $\gamma$  between any pair of outwards direction vectors and the cardinality  $|E_1|$  of the set of outwards direction vectors  $E_1$  related to the current critical region  $s_1$ . (a) If a critical region presents  $|E_1| = 2$  and  $\beta < 90^\circ$  it is immediately classified as a bifurcation 1; (b) if  $\beta \geq 90^\circ$  it may be a bifurcation 2 or (c) even a bifurcation 3 as long as there is another critical region nearby. (d) A bifurcation 4 presents  $|E_1| = 3$ , but there is no  $\gamma \approx 180^\circ$ . (e) A superposition appears with  $|E_1| = 2$  and another critical region  $s_2$  nearby, with  $\gamma \approx 180^\circ$ . (f) Finally, a crossing has  $E_1 = 3$  and  $\gamma \approx 180^\circ$ . Notice that bifurcation 1 could be mistaken for either bifurcation 4 or superposition and bifurcation 2 could be mistaken for bifurcation 3 in case the adopted rules had not been considered.

must be taken. In addition to finding the optimal segment to move ahead, the algorithm also identifies the current critical region as either a bifurcation, a superposition or a crossing. If the current critical region is a bifurcation, the *BTA* stores the related secondary seed in an auxiliary queue, otherwise the *BTA* stores the addresses of the current segment end point and the next segment starting point. By doing so, the *BTA* labels all the segments comprising each dendritic branch in a recursive-like fashion, until reaching a termination.

- **Branching Structure Contour Extraction Algorithm.** The **BSCEA** main role is to extract the parametric contour  $c(t) = (x(t), y(t))$  along the segments comprising a 2D neuron image by using the labeled branches and classified critical regions obtained in the previous step. Basically, the *BSCEA* follows the segments defining branching structures (resulting from the union between the labeled skeleton and the soma) by entering all the shape innermost regions. During the contouring process, whenever a branching region is found, the *BSCEA* contours the shape

outwards, as the traditional algorithm would. On the other hand, whenever a crossing or a superposition is found, the *BSCEA* contours the shape inwards, by traversing the current critical region through the addresses stored in pointers by the *BTA*. Finally the *BTA* gives as a result the contour parametric functions  $x(t)$  and  $y(t)$  as well as a contour image (Fig.16(b)).

These procedures are detailed in Sections 3.1, 3.2 and 3.3, respectively.

### 3 General Framework

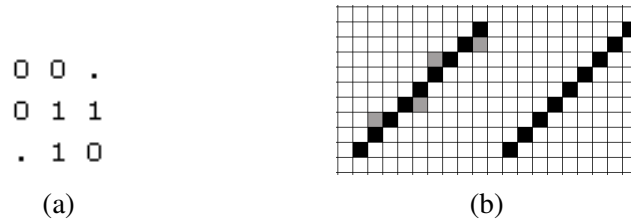


Fig. 5. (a) Hit-or-Miss template used to filter the pruned skeleton, resulting in an 8-connected skeleton with one-pixel wide branches. (b) The light shaded pixels at the left-hand side must be removed yielding the essential structure at the right-hand side.

#### 3.1 Preprocessing

Some important shape parts are detected by taking into account specific features, such as the number of each pixel’s neighbors and the size of the shape. For example, pixels of branches are expected to have only 2 neighbors each, while critical regions and the soma have more. Moreover, the soma area is greater than the areas of the critical regions.

Initially, a preprocessing pipeline involving mathematical morphology transformations <sup>2</sup> is carried out on the input image, so as to obtain the separate components of the neuron image, that is the skeleton comprised of 8-connected one-pixel-wide branches, the critical regions, the terminations, the soma and the queue of primary seeds. The referred separate components on different images are obtained as described in the flowchart diagram depicted in the Fig. 6.

All the used structuring elements are flat and centered at their origins, i.e. their centroids.

In order to isolate the soma, the image is eroded by a disk with radius 3, followed by a dilation with a disk with radius 1. It is known that soma shapes do not follow

<sup>2</sup> The reader is referred to [10,24] for details on the mathematical morphology operations.

a clear pattern, making their segmentation critical. Herein, the soma segmentation is attained through erosion, noise filtering by area opening, followed by a dilation. Casual noisy pixels surrounding the soma image are wiped out through the skeleton area opening. Then, additional processing is applied in order to obtain an 8-connected skeleton with one-pixel wide branches [16](??).

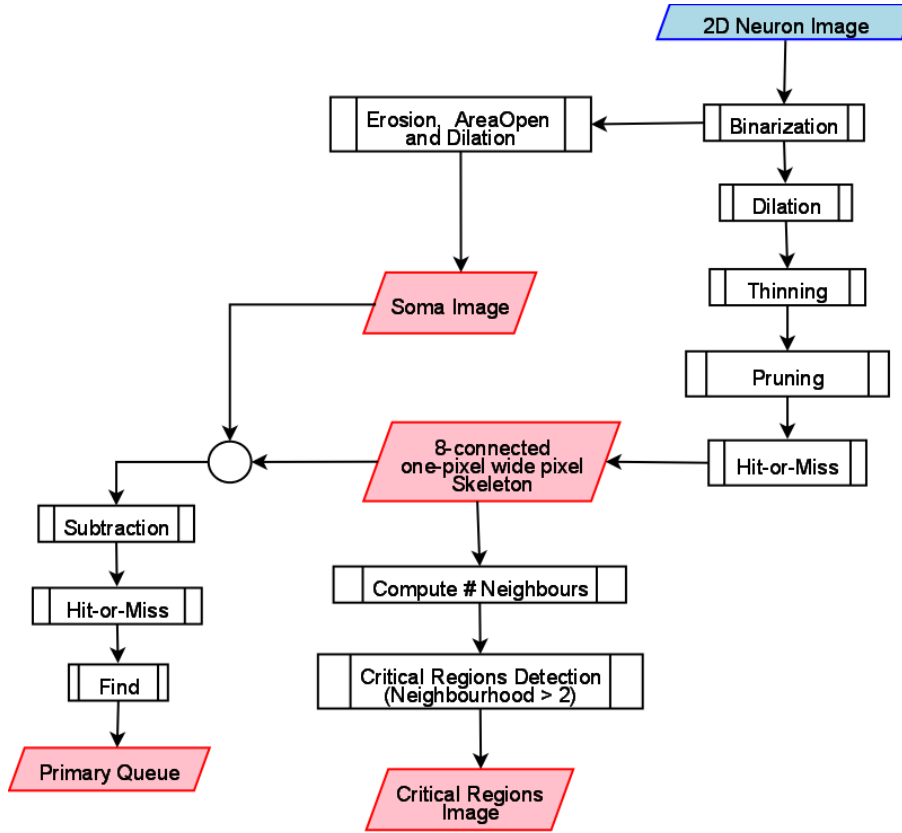


Fig. 6. Flowchart of the preprocessing pipeline. The red polygons represent the outcomes.

The most critical and perhaps difficult template to define would be that portrayed in Fig. 5 for the Hit-or-Miss operation. The Hit-or-Miss is a mathematical morphology operation [10], being a sort of loose template matching, because the template itself is an interval, instead of a specific shape. Whenever certain small structure present on the image fits inside this interval, it is marked. Herein, the Hit-or-Miss operation is applied using the template depicted in Fig. 5(a) to detect redundant skeleton pixels which should be ruled out, as shown in Fig. 5(b).

### 3.2 Tracking of Branches

One of the main goals at this stage is to label each dendritic branch as a whole object on its own. This is achieved by pixel-by-pixel labeling of each branch. Considering the sequential nature of such a processing, this problem may be described as estimating the spatial coordinates  $(x, y)$  of each subsequent branch pixel. Be-

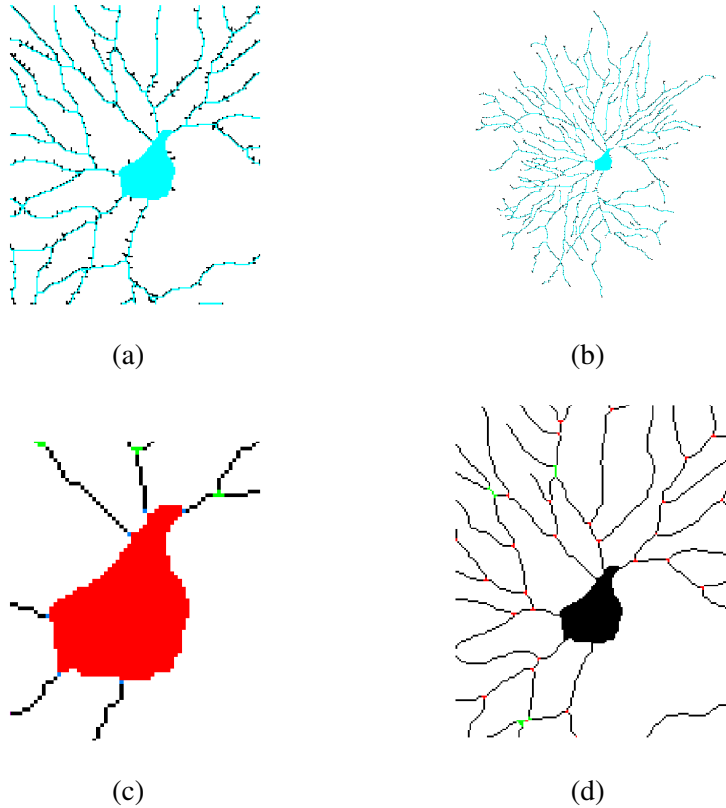


Fig. 7. Preprocessing results: (a) The darkest pixels were removed by the *Hit-or-Miss* filtering yielding the 8-connected skeleton with one-pixel wide branches shown in lighter cyan; (b) Pruned 8-connected skeleton (cyan) with one-pixel wide branches superimposed to the skeleton (black); (c) Soma (red), seeds (blue), critical regions (green) and skeleton (black); (d) Critical Regions (green and red) and skeleton (black).

cause this is analogous to tracking problems [1] in the computer vision literature, this algorithm is called *Branches Tracking Algorithm (BTA)*.

*Tracking* is usually divided into *Prediction*, *Measure* and *Update* stages [1]. During the *Prediction* stage, the algorithm estimates the next state of the system. On the *Measure* stage, the algorithm probes the system by looking for plausible states nearby, in this case valid pixels, through some measures, herein the spatial coordinates  $(x, y)$  of pixels. During the *Update* stage, the algorithm merges both pieces of information gathered on the previous two stages, through a linear combination, giving as a result the optimal estimation for the next state. So, in terms of *Tracking*, the *BTA* *Prediction* and *Measure* stages are carried out in a single step, through the 8-neighborhood scanning by using the chain-code [8].

The *BTA* *Update* stage is related to the pixel labeling. This stage labels each dendritic subtree growing out of the soma in the same way, i.e. by starting from the related primary seed and labeling the entire branch adjacent to it, up to its termination. Meanwhile, its branches are marked to be labeled afterwards. Thereafter, every

branch is labeled as the first branch was, and the respective encountered branches are similarly marked to be labeled afterwards in a recursive-like fashion until the whole dendritic subtree is labeled.

The *BTA* is mainly composed of two nested loops. The outermost loop is on primary seeds, being related to the labeling of each dendrite having root in the soma. The innermost loop is on secondary seeds, being related to the labeling of each branch within a given dendrite. This algorithm is depicted in the flowchart of Fig. 8. It is worth mentioning that, for our purposes, valid pixels are defined as simultaneously non-labeled and non-critical foreground pixels. Then, for each primary seed, the *BTA* starts by subsequently stacking every valid pixel from a segment to be labeled afterwards, until either a termination or a critical region is reached.

On arriving at a critical region, the *BTA* may perform one or two of the following tasks, *Continuity of the Tangent Orientation Assessment* and *Critical Regions Classification*. The former (detailed in the Section 3.2.1) is always carried out, while the latter (described in the Section 3.2.2) is performed only if the current critical region has not been classified yet. Notice that though the critical regions are now available from the previous preprocessing step, they are not classified yet, i.e. we do not know which is a bifurcation, a crossing or a superposition. This classification is important for the contour extraction step.

### 3.2.1 Continuity of the Tangent Orientation Assessment

Analogously to the tracking process during branches labeling as described in 3.2, this step also comprises Prediction, Measure and Update, however in a slightly different fashion. Coming to a critical region in this step is similar to approaching the occlusion case in tracking problems [11], where different objects follow trajectories which apparently overlap.

So, after arriving at a critical region, the Prediction stage is performed by computing the *inwards direction vector*  $\hat{v}_0$ . In the Measure stage the algorithm calculates all *outwards direction vectors*  $\hat{v}_i$ . Finally, in the Update stage the outcomes from the Prediction and Measure stages are merged. The reason to do that is to estimate the best candidate segment among all the alternatives so as to carry forward the tracking procedure. This merging is achieved by the calculation of inner products (projections) between the inwards direction vector  $\hat{v}_0$  and each outwards direction vector  $\hat{v}_i$  (observe that these two vectors have unitary magnitude), according to Eq. 1:

$$k = \arg \max_i (\langle \hat{v}_0, \hat{v}_i \rangle) \quad (1)$$

where the index  $k$  is assigned to the direction vector  $\hat{v}_k$  among  $\hat{v}_i$ , for which the

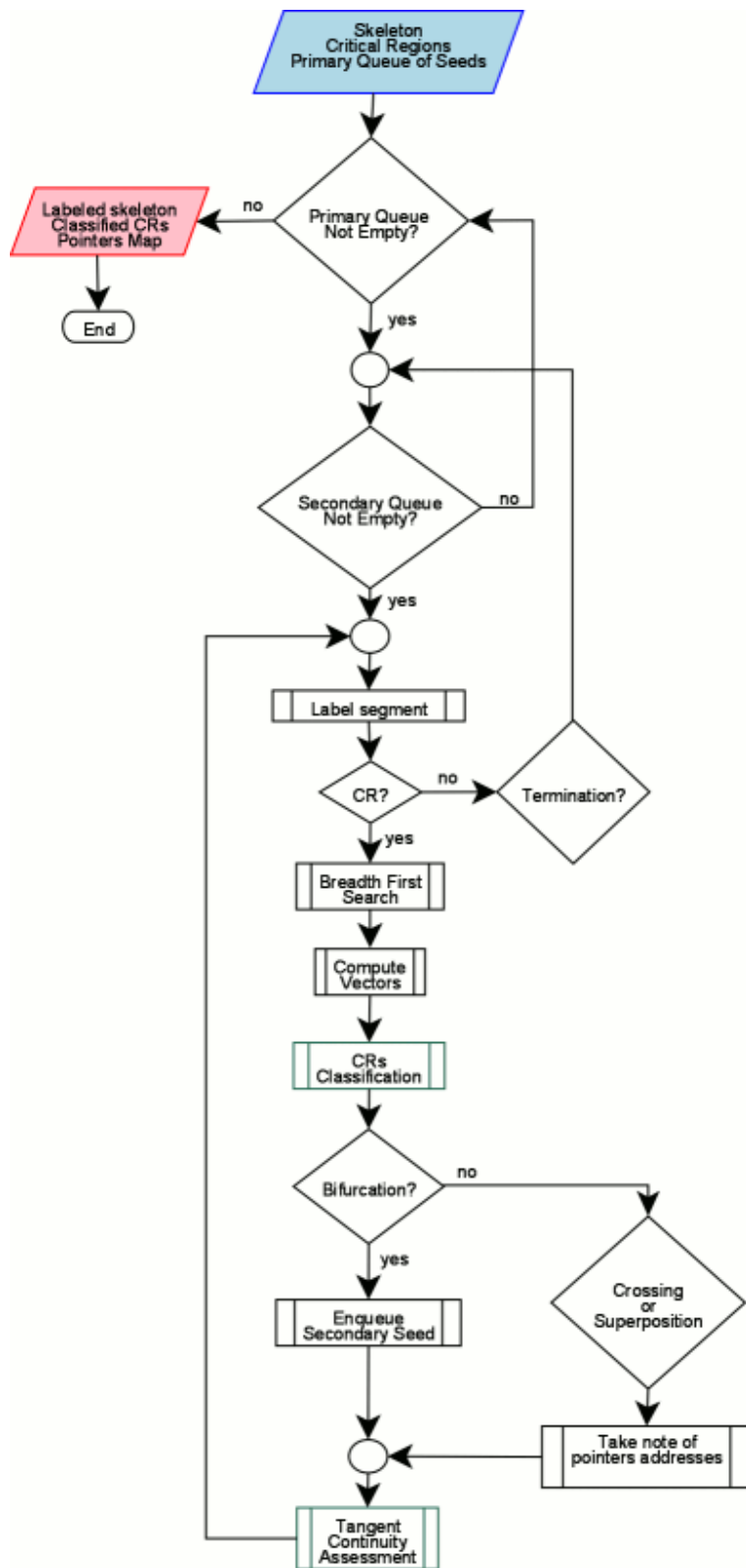


Fig. 8. Flowchart of *BTA*.

inner product result is the largest. The extremity points for properly computing each vector are determined through a *Breadth-First Search* approach <sup>3</sup>.

Every time a critical region is encountered, the Breadth-First Search is triggered and all the forward neighboring pixels are iteratively enqueued into an auxiliary queue, while passing across the just detected critical region. At each Breadth-First Search iteration, the auxiliary queue is run through in search of critical pixels. The stop condition for the Breadth-First Search is set beforehand as a number  $C$  of consecutive executions through the auxiliary queue without finding any critical pixel. This procedure is detailed in an example in Appendix A.1.

The starting pixel of the optimum segment to proceed is lastly stacked and labeled. Also, the alternative path origin is considered as a secondary seed, that is a side branch seed to be enqueued in case a bifurcation is detected. Conversely, in case either a superposition or a crossing is detected, the next segment starting point  $V_{n+1}$  and the current segment last point  $V_n$  (Fig. 13(b)) addresses are stored into the Pointers Map.

### 3.2.2 Critical Regions Classification

While assessing the orientation of the tangent direction vectors at each critical region, as described in section 3.2.1, the *BTA* also gathers enough information to classify the current critical region into one of the 6 different classes (see Fig. 4), which have been identified as being critical for the skeletons. *Critical Regions Classification* is a crucial concept for the proper functioning of our *Contour Extraction* algorithm presented in section 3.3. Although *Critical Regions Classification* is not an algorithm on its own, it is an important part of the *BTA*. Therefore, each critical region is classified according to some special rules. The decision tree depicted in Fig. 9 details both the classification rules themselves and the order in which they should be considered, i.e. it illustrates the flow of decisions required to properly classify a critical region into one of the 6 classes showed in Fig 4. These classes have been abstracted from the analysis of several images, during the development of our methodology. We started from the assumption that  $2D$  branching structures are comprised of only bifurcations 1 and crossings. So the number of adjacent segments (3 or 4) at every critical region should be enough to classify them. However, misclassifications during the system development implied a more complete description. The system became more and more robust, as we moved further by taking into account new pieces of information, such as orientation between incoming and outgoing direction vectors, proximity relation between neighbor crossing regions, besides the basic and first criterion of number of adjacent segments to each crossing region.

---

<sup>3</sup> The Breadth-First Search is a suitable method to find the shortest path between two nodes in a graph, implemented by using a queue of nodes as a data structure [23].



In brief, the critical regions classification rules take into account the angle  $\beta$  between the inwards direction vector -  $\hat{v}_0$  - at the current critical region  $s_1$  and its outwards direction vector -  $\hat{v}_2$ ; the angle  $\gamma$  between any pair of outwards direction vectors  $\hat{v}_i, \hat{v}_j$ ; and the cardinality  $|E_1|$  of the set of outwards direction vectors  $E_1$  related to the current critical region  $s_1$ .

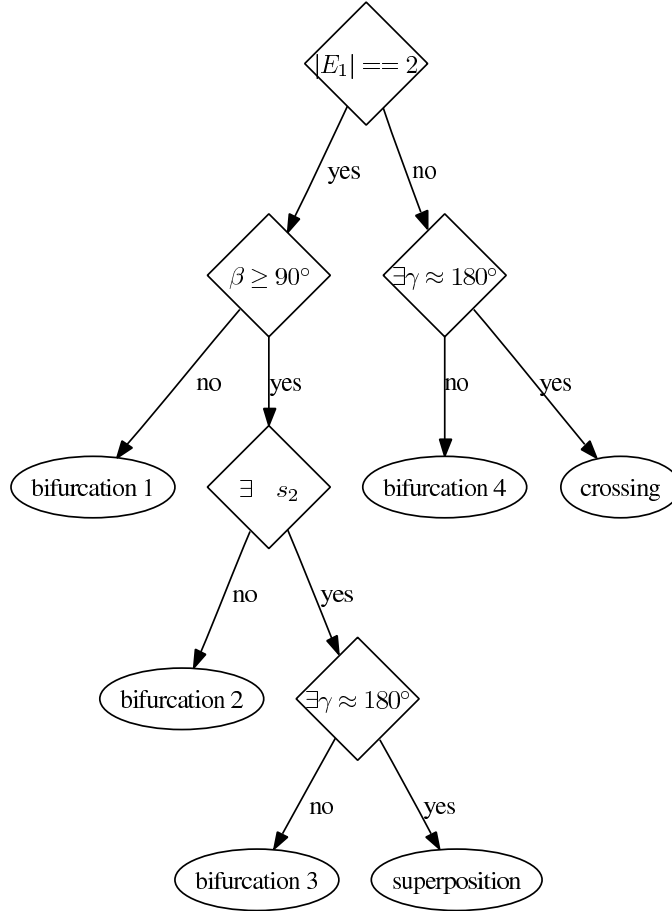


Fig. 9. Decision tree representing the sequence of rules applied for Critical Regions Classification by the **BTA**. The variables  $s_1$  and  $s_2$  represent respectively the current critical region and other nearby in the set  $S$  of critical regions (see Fig. 4). The variables  $E_1$  and  $E_2$  stand for the sets of unitary **outwards vectors** related to  $s_1$  and  $s_2$  respectively. Since a critical region is individually classified as it is found during the labeling process, it is clear that the current critical region  $s_1$  exists. The variable  $\beta$  measures the angle between the inwards direction vector and the outwards direction vector, while the variable  $\gamma$  measures the angle between any two outwards direction vectors. Refer to the Appendix A.2 for further explanation on notations.

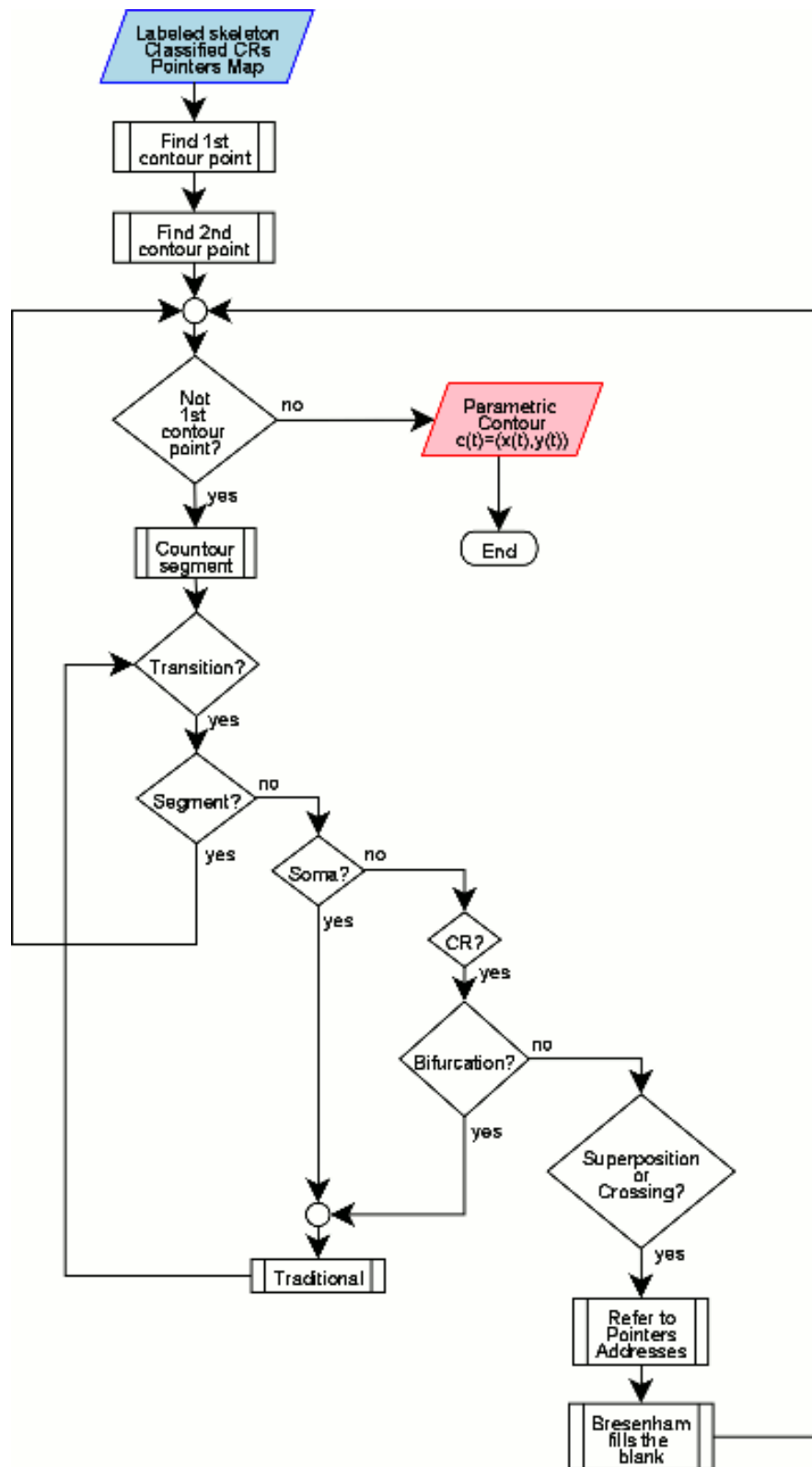


Fig. 10. Flowchart of the *BSCEA*.

### 3.3 Contour Extraction

Consider the following conventions for the *Branching Structures Contour Extraction Algorithm* (**BSCEA**) description:

- i input: union of labeled skeleton and soma images.
- ii directions related to the current  $C$  pixel are identified according to the chain-code.
- iii the input is followed in a counter-clockwise sense.
- iv all the  $N$  points of the parametric contour are stored in a suitable data structure  $E(1..N)$ . Each element  $E(n)$  keeps the  $n^{th}$  contour point coordinates, i.e.  $E(n).x$  and  $E(n).y$ , which are the computational representation for  $x(t = n)$  and  $y(t = n)$  respectively. When the contour is closed,  $x(t = 1) = x(t = N)$  and  $y(t = 1) = y(t = N)$ .

The main steps composing the *BSCEA* are depicted on the respective flowchart in Fig. 10. The contour following algorithm explained in [8] has been adopted in this work.

#### 3.3.1 Finding the first pixel

The **BSCEA** starts by a raster scanning, i.e., from left to the right, from top to the bottom, in search of the first contour pixel  $E(1)$ , which should be the first background pixel found that is also a neighbor of a foreground pixel. In the sequel, the *BSCEA* will contour the shape all the way, until coming back to the first pixel, closing the cycle and having  $E(1) = E(N)$ .

#### 3.3.2 Finding the next pixel

From the second pixel on, the chain-code will be used to scan the current pixel vicinity. In so doing, the second contour pixel will be the first neighbor in the chain-code sequence 4, 5, 6, 7, 8, which is also a background pixel and a neighbor of a foreground pixel. Herein this scanning in search of the next pixel is done analogously to that by the traditional contour extraction algorithm [8]. Besides direction relationship between *current* and *previous pixels* (see Fig.11) to properly decide about the next contour pixel, it shall be considered the transition between labels, so as to know if the *BSCEA* is contouring a branch, the soma or a critical region. The *BSCEA* contouring strategy is in accordance with the specific structure being contoured. So, the main *BSCEA* parameters are:

- the current contour pixel  $E(n)$
- the direction  $d_{cp}$  from the current to the previous pixel
- the previous pixel label

- the current pixel label

Providing the *BSCEA* with the  $E(n)$  pixel and direction  $d_{cp}$  allows the identification of the starting point to scan the neighborhood in search of the next pixel [8], according to the chain-code sequence.

Since the input for the *BSCEA* is a union of the labeled skeleton and the soma images, it is necessary to adopt a policy to properly find the next pixel in each case. Hence, the *BSCEA* considers contouring branches as the default case, taking the first background pixel which is also neighbor of a foreground pixel in the neighborhood defined by the chain-code. Conversely, the *BSCEA* considers contouring the soma as a particular case, taking the last pixel, instead of the first one, to be included as contour. By so doing, the *BSCEA* is able to contour branches, while preserving the ability of more traditional approaches to circumvent the problem of contouring occasional one-pixel wide entrances into the soma, consequently allowing the contour to be closed [8].

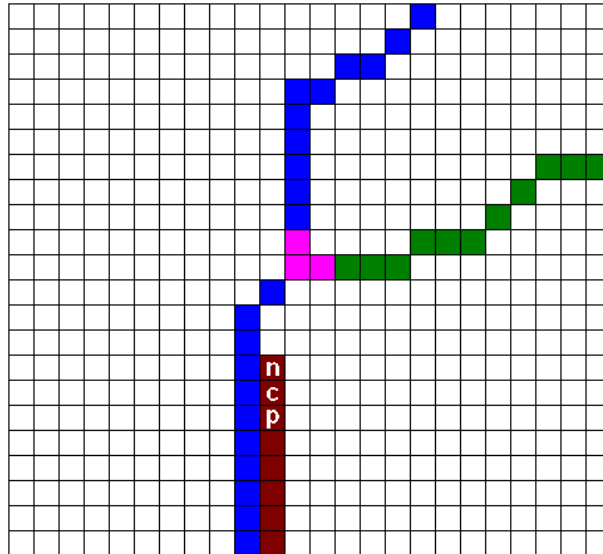


Fig. 11. Previous (**p**), Current (**c**) and Next (**n**) pixels represented in an iteration of the *BSCEA*. The direction relationship  $d_{pc}$  between the pixels **p** and **c**, besides the labels assigned to the segments, determine the Next pixel **n**.

### 3.3.3 Traversing critical regions

It is also necessary to devise a strategy for critical regions processing, according to their classes, as described in section 3.2.2. Regions classified as Bifurcation should be contoured outwards, while those ones classified as either Superposition or Crossing should be contoured inwards, through pointer addresses written to the *Pointers Map* data structure during the tracking stage. The integration between soma and labeled skeleton is critical for the successful contour extraction, since it guarantees the contour closing.

The *BSCEA* can deal with both cases by taking into account the labels of previous and current pixels, which convey valuable information concerning particular situations, i.e. if the critical region is a bifurcation, "contour it outwards" (see Fig. 10 and Fig.12), as well as the traditional contour extraction algorithm would [8]. In case it is a superposition or a crossing, "contour it inwards", (see Fig. 10 and Fig. 13), which means to trace a line between the current segment end point and the next segment starting point. Both points are known from the pointers marked by the *BTA*. The line is traced by using the Bresenham algorithm [2] for tracing a digital straight line segment.

- *case 1: BSCEA* is contouring some branch
  - take the 1<sup>st</sup> candidate in the chain-code sequence.
- *case 2: BSCEA* is at a transition between a branch and the soma
  - take the last candidate in the chain-code sequence.
- *case 3: BSCEA* is at a transition between a branch and a critical region
  - (a) if the critical region is a bifurcation, "contour it outwards" (see Fig. 10 and Fig.12).
  - (b) if the critical region is either a superposition or a crossing, "contour it inwards", (see Fig. 10 and Fig. 13).

In the case 3-a, "contour outwards" means contouring the shape as the traditional contour extraction algorithm would [8], as shown in Fig.12.

In the case 3-b, "contour inwards" means:

- probing the current pixel  $E(n)$  vicinity in search of the respective pointer  $P_n$  in the *Pointers Map* data structure
- determining the direction relationship  $d_{E(n) \leftrightarrow V_n}$  between  $E(n)$  and the current segment end point pixel  $V_n$
- accessing the next segment starting pixel  $V_{n+1}$ , pointed to by  $P_n$
- assuming  $d_{E(n+1) \leftrightarrow V_{n+1}} = d_{E(n) \leftrightarrow V_n}$  and finding  $E_{n+1}$  accordingly
- filling the blank in the contour over the critical region with a digital line between  $E(n)$  and  $E(n + 1)$ , by using the Bresenham's algorithm [2].

Notice that the *BSCEA* cannot tell which pixels of a superposition or crossing are related one another or to a branch, since the projection from the 3D neuron onto the 2D plane suppresses this information. Such a problem is circumvented by replacing the shared pixels in the critical region by two short intercepting segments given by the Bresenham's algorithm, as illustrated in Fig.13.

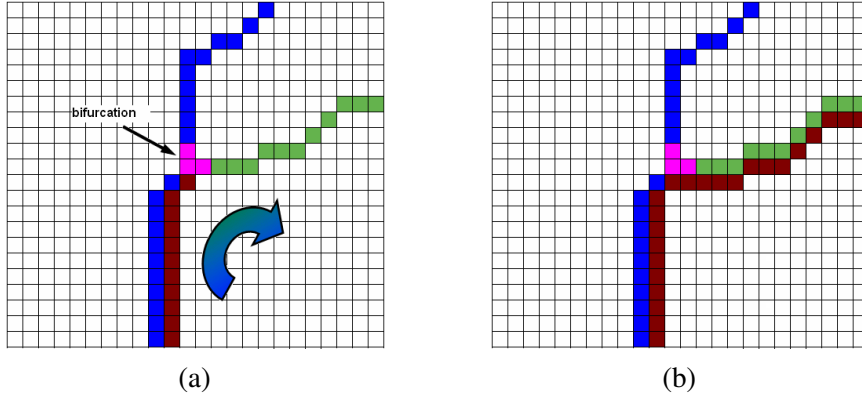


Fig. 12. Contouring a bifurcation. Branches appear labeled in blue and green, while the critical region previously classified as a bifurcation appears in magenta. The contour is shown in brown. (a) By detecting labels transition, the *BSCEA* identifies that it has arrived at a bifurcation, thus deciding to contour the shape outwards. (b) Having left the critical region behind, it proceeds until reaching another critical region.

## 4 Results

All the methods described in this work have been implemented as *Matlab*<sup>®</sup> scripts, using the *SDC Morphology Toolbox for MatLab*<sup>™</sup> [13]. The overall method has been evaluated with respect to a data set containing several images of ganglion cells in the retina of cats, acquired by camera lucida. In order to reflect an important biological investigation, we have chosen *2D* neuron images from [18].

Results obtained for three images were chosen to be presented in this work. Figure 14 shows labeled neuronal images (right column) obtained from alpha, delta and epsilon (left column) types of neurons. New labels were assigned to dendrite segments originating from branches. The algorithm is able to distinguish between critical region classes, reflected by the correct assigned labels for the outwards segments from such structures. Notice how the cases of close parallelism imply the *BTA* to label the clumped segments as superposition regions. Moreover, long overlaps are also labeled as superposition regions, as long as such an overlap is smaller than  $D_{max}$ , which is the minimum path length allowed between two critical regions. Extremely close bifurcations of type 1 can be labeled as a bifurcation of type 4. All the bifurcations, superpositions and crossings have been correctly labeled.

Results for the *Branching Structures Contour Extraction Algorithm* are presented in Figure 16, where one can see the parametric contour trace for the shape and a comparison between the results obtained by using both the traditional and the *BSCEA* approaches. Observe from Figures 16(a), 16(c) and 16(e) how the traditional algorithm did not afford access to the innermost neuron contour portions, while the *BSCEA* conversely ensured full access to all neuronal processes, as shown in Figures 16(b), 16(d) and 16(f).

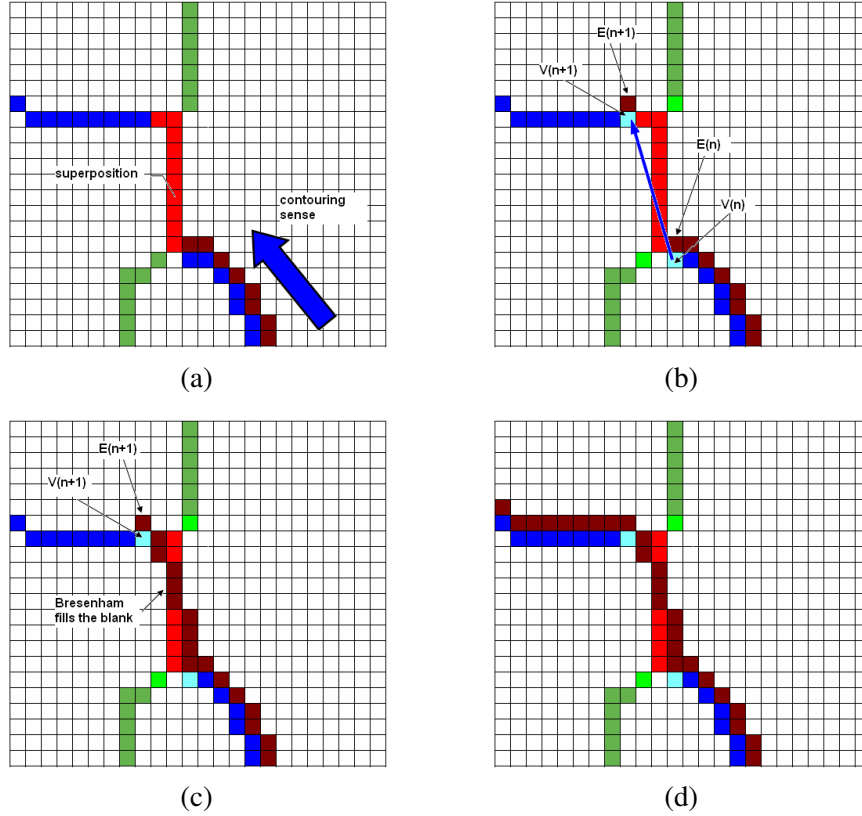


Fig. 13. Contouring an overlap. Branches appear labeled in blue and green, while the critical region previously classified as a superposition appears in red. The contour is shown in brown. (a) By detecting labels transition, the *BSCEA* identifies that it has arrived at an overlap, thus deciding to contour the shape inwards. (b) Firstly the *BSCEA* looks in the vicinity for the pointer  $P_n$ , related to the current segment end point pixel  $V_n$ . The pointer  $P_n$  stores the address of the next segment pixel beyond the critical region, namely  $V_{n+1}$ . Subsequently the algorithm determines the direction relationship  $d_{E(n) \leftrightarrow V_n}$ . Assuming  $d_{E(n+1) \leftrightarrow V_{n+1}} = d_{E(n) \leftrightarrow V_n}$ , it finds the next segment starting pixel  $E(n+1)$ . (c) The Bresenham's algorithm is applied to trace a digital line between  $E(n)$  and  $E(n+1)$ , filling the blank in the parametric contour signal over the *critical region*. (d) Having left the critical region behind, it proceeds until reaching another critical region.

Additional experiments have been carried out in order to validate the algorithms and to assess their performance with respect to noisy neuronal images. A validation test was performed with a synthetic neuron image, by labeling it manually and automatically through the *BTA* (Fig. 18). Despite differences between manual and automatic labelings, due to distinct assessments of tangent continuity for some bifurcations in both approaches, notice that both labelings are consistent, providing suitable input for the *BSCEA* which yielded identical parametric contours for both labelings. The robustness of the proposed methodology for noisy versions of the same synthetic neuron image has been tested by convolving the original synthetic image with six different *2D* Gaussians, using bandwidths parametrized by values of standard deviations spanning from  $10^{-8}$  up to  $2 \cdot 10^{-6}$  in the Fourier domain. Figure 19 shows results for extreme cases, namely the original synthetic image and

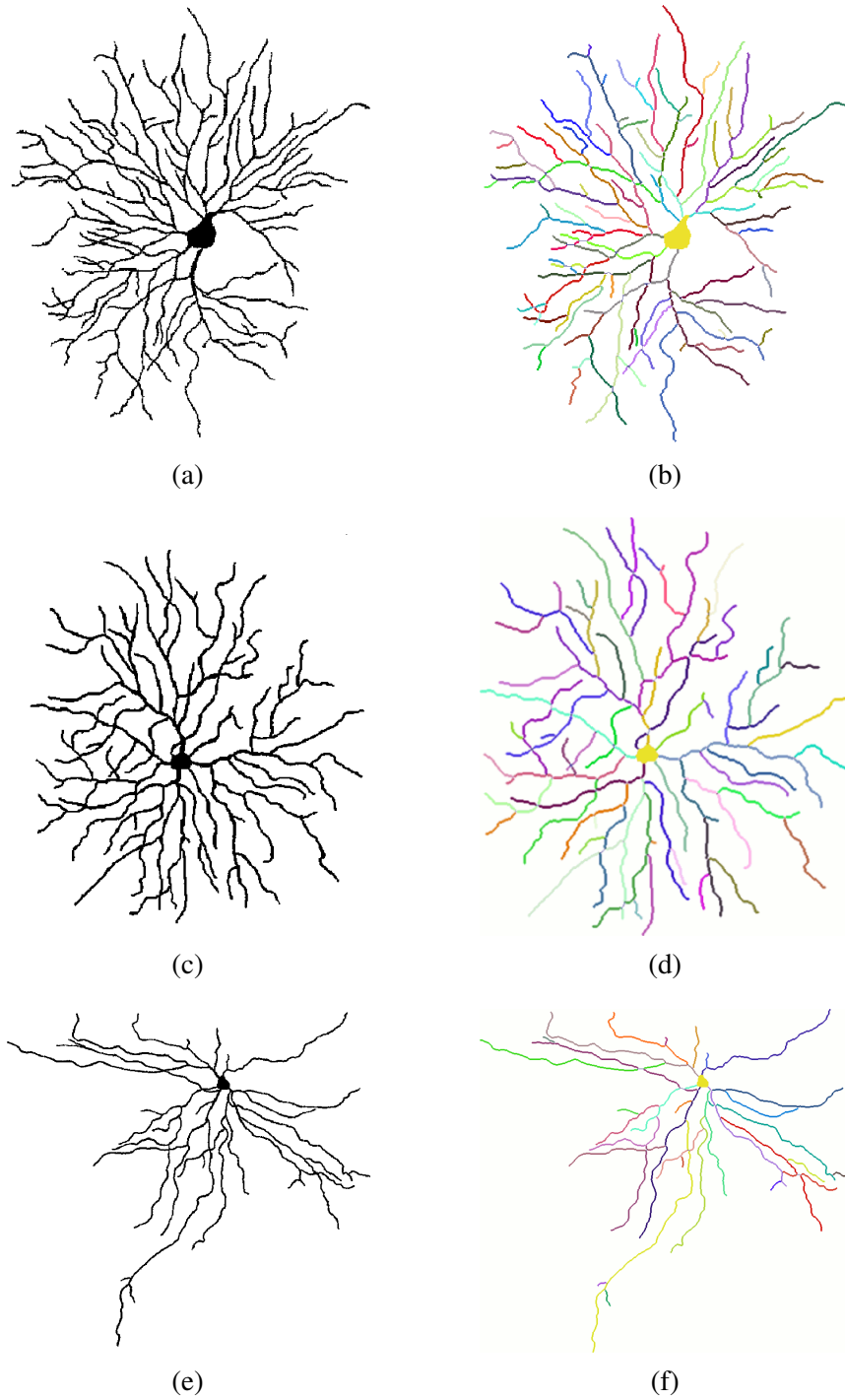


Fig. 14. Results obtained by the *Branches Tracking Algorithm* when applied to alpha, delta and epsilon neuron images. (a) Alpha (c) Delta and (e) Epsilon neuron images and respective labeled images in (b), (d) and (f). Distinct branches appear in different colours.

the smoothest version of it. Notice that the *BTA* provided consistent labelings for the original and the smoothed versions, and the *BSCEA* yielded identical parametric contours for both cases.



## 5 Concluding Remarks

The proper shape characterization of branching structures is a particularly important problem, as it plays a central role in several areas of medicine and biology, especially in neuroscience. Indeed, the current understanding of the physiological dynamics in biological neuronal networks can be reinforced through the proper characterization of neuronal cells shapes, since both the amount of synapses and the way in which neurons organize in networks are strongly related to the cells shapes.

Local information is retrieved through parametric contour analysis, while global information can be acquired from statistical measures considering the shape of the whole cells. However, accurate contour following in neuronal shapes has not been possible so far because of the presence of overlappings among neuronal processes implied by the projection from  $3D$  neuronal shapes onto  $2D$  images. Whenever a crossing takes place in these images, the traditional contour following algorithm, which is based on the chain-code, fails to enter their innermost regions. The present work described an original methodology capable of properly tackling the problem of following the contour of branching structures, even in the presence of intercepting branches. The main original contributions of our method<sup>4</sup> include both the tracking of the branching structures, such as neurons, as well as the extraction of the respective parametric contours. In addition, the features adopted in this work to classify critical regions – such as shape, number of adjacent segments and angles among segments, have intrinsic potential for providing additional information to be used in neuronal characterization and classification. Our system is basically comprised of three parts, i.e.: (i) *Preprocessing Algorithm*, (ii) *Branches Tracking Algorithm - BTA* and (iii) *Branching Structures Contour Extraction Algorithm - BSCEA*.

Because the proposed system begins with a series of transformations (preprocessing) on the  $2D$  projection of a  $3D$  branching structure image, so as to obtain a suitable skeleton, obviously any skeletonization scheme other than the morphological thinning might be adopted, such as exact dilations [8], medial axis transform, and so on, provided that an 8-connected skeleton with one-pixel wide branches is obtained as a result. Besides, the skeletonization scheme will affect the choice of all the preprocessing parameters, which in this work have been picked out by trial and error. One should bear in mind that the method gist is supplying the tracking algorithms with an adequate skeleton as input.

Apart from the skeleton, there are a number of separate components obtained through the preprocessing step. Although the data structure to store such separate components is immaterial to the preprocessing pipeline implementation, since it may be implemented in alternative ways, we particularly have them separated and stored

---

<sup>4</sup> Preliminary results of the proposed approach have been described in conferences ([15, 17]).

into separate images, for the sake of easier implementation. As will be shown in the sequel, the system dynamics involves comparisons among such pieces of information, which may be properly achieved by means of set operations (union, intersection, set difference, etc). Considering that mathematical morphology operations are usually described in terms of set operations (union, intersection, etc.) and that the *SDC Morphology Toolbox for MatLab*<sup>™</sup> [13] implements such operations, we decided to take advantage of it by separating those structures into different images. However, instead of separating structures in images, one could label a pixel pertaining to a structure, by using the Object-Oriented Programming Paradigm to keep such information in the respective pixel attribute. Moreover, it should be emphasized that the one-pixel-wide restriction on the branches of the skeleton is mandatory in order to guarantee the proper operation of the tracking algorithm. In general, the dendritic tree should be one-pixel wide, because the tracking procedure is based on the stacking of nearby valid (background, unlabeled) pixels, following the chain code order. Hence, the thicker the structure, the larger the number of pixels in the vicinity of the current pixel. These irrelevant pixels would be indistinctly staked, putting the BTA in a forward-backward visitation of pixels, and not in a sequence. One should bear in mind that a one-pixel wide skeleton gathers enough information concerning the essential structure of the shape [8].

Notice that the structuring elements dimensions have been obtained in an empirical basis, specially for the images used in this work. Three images have been used to calibrate these parameters: an *alpha* neuron image of size  $500 \times 598$ , a *delta* neuron image of size  $475 \times 511$  and an *epsilon* neuron image of size  $768 \times 712$ . It should be emphasized that images with very different sizes may require different structuring elements. Considering that Mathematical Morphology Image Processing depends on the structuring element sizes and shapes, choosing a suitable structuring element is important. Therefore, for different sized images from the mentioned above, one will have to test disks with different diameters, following the sequence of operations described.

The algorithms robustness regarding the contrast in input images is not affected, since the preprocessing first step is to binarize the input image. Also, for the purposes of this methodology, noise is related to redundant pixels, such as those wiped out through the hit-or-miss filtering operation.

As for the *BTA*, there may be particular cases for further consideration yet, for example images with high density values of critical regions and/or the presence of structures whose topologies might favour the appearance of superpositions. The first case, i.e. high critical regions densities may be due to particular shape topologies in the image or due to the image resolution itself, causing the *BTA* to cluster critical regions occurring very close to one another. Notice that, in an effort to fulfil the previously set stop condition for the Breadth-First Search, the *BTA* has bunched both bifurcations of type 1 (Fig. A.3-(a)) into a cluster of bifurcations appearing as a bifurcation of type 4 (Fig. A.3-(b)). A possible solution is to use breadth-first

search implemented with a tree data structure, in addition to the auxiliary queue, in order to properly maintain memory of valid paths between direction vector terminations and origins. Immediately after achieving the stop condition, the *BTA* would retrieve the direction vectors end points hosted at the tree leaves. The respective direction vectors origins would simply be obtained by climbing the tree from the leaves upwards, until reaching the respective first non-critical pixels adjacent to the precedent critical region. Moreover, this strategy might allow disambiguating between two possible origins that are equally far apart from a very same direction vector termination, since the shortest distance between a direction vector termination and an origin candidate is the only condition taken for granted. The auxiliary tree data structure would add a piece of information regarding the existence of a valid path (segment) between a direction vector termination and an origin candidate.

In the second case, that is Superpositions, one should notice that such regions may be resultant from three distinct problems. Firstly the hugely close parallelism, in which images containing many branches almost parallel and very close to each other usually come to present short cycles after the preprocessing stage. Short cycles are highly undesirable, since they are error-prone structures. This problem may be circumvented by including a dilation step in the preprocessing pipeline, just before the skeletonization. In so doing, short cycles are shrunk into closed Superposition regions. Secondly, poor resolution may yield images having ellipsoid cigarshaped crossings sampled as almost line-shaped structures. After the preprocessing, these structures will appear as Superposition regions. Lastly, long overlaps will also be labeled as superposition regions, provided that such overlapping is below the threshold  $D_{max}$ , that is the shortest allowed path length between two bifurcations.

Needless to say that the system performance should not be evaluated on the basis of the number of images, but rather on the number of fully accomplished tasks. Regarding the number of successful objects processed, the number of trespassed critical regions, during the contour following process, is a quantitative assessment *per se*. Notice that the parametric contour following process is a sequential procedure, in which any mistake will prevent the algorithms to continue and reach their goal. In the case of *BTA*, the task is to label every branch. In the case of *BSCEA*, the task is to obtain the parametric closed contour, coming back to the first pixel it started from. Having this in mind, *BTA* succeeds only and if only if it does not leave any branch out without being labeled. So the more labeled branches within a neuron, the more evident the *BTA* success. As for the *BSCEA*, it succeeds only and if only if it could return to the first pixel it started from, after having the whole pattern contoured. So, the more critical regions within a  $2D$  neuron image, the more evident the *BSCEA* success. Also, concerning the quantitative validation between results obtained from the traditional and the *BSCEA* approaches, Fig. 17 displays the parametric signals  $(x(t))$  and  $(y(t))$  for both cases. Several global features may be calculated from these signals, such as the bending energy.

The most expensive operation in the BTA would be to check every pixel at some 8-neighborhood to decide whether or not it should be labeled. However this is done at most a constant number of times. So, tracking would be eventually of  $O(n)$  with respect to the number of object pixels (far less than the size of the image). Similarly, in BSCEA, every pixel in the neighborhood of a labeled pixel is visited to check whether it has a blank neighbor which will ultimately become a contour pixel, so it would also be of  $O(n)$ .

The main original contributions of the present work<sup>5</sup> encompass both the tracking and the parametric contour extraction from branching structures, like neuron cells. Future developments include the extension of the methodology to separate cells in images containing multiple cells. Several applications of the methodology proposed in this work can be made regarding neural networks images as well as other types of biological structures such as retinal vessel trees.

---

<sup>5</sup> Preliminary results of the proposed approach have been described in conferences ([15, 17]).

Table A.1

Breadth First Search across a bifurcation of type 1: auxiliary queue states.  $B$  is set to 1 whenever every pixel in a specific state is non-critical and 0 otherwise.  $\Sigma$  increases by one if the respective  $B$  variable has been set to 1, and zeroed otherwise. Already dequeued pixels have been concealed.

state	current	auxiliary queue	B	$\Sigma$
00	a	b	0	0
01	b	c d	0	0
02	c	d e	0	0
03	d	e f	1	1
04	e	f g	1	2
05	f	g h	1	3
06	g	h i	1	4
07	h	i j	1	5

## A Appendices

### A.1 Breadth-First Search Example

This process is illustrated in Fig. 1(a) which is related to Table A.1, Fig. 1(b) and Table A.2. The former example illustrates the *Breadth-First Search* across a single bifurcation, while the latter example illustrates the Breadth-First Search across two very close bifurcations, giving rise to the agglutination effect of two bifurcations of type 1 (Fig. 4(a)) into one bifurcation of type 4 (Fig. 4(d)). In both examples one may realize that the state 0 has been obtained by probing the vicinity of the pixel **a**, in the chain-code (Fig. A.2) sequence 3, 4, 5, 6, 7, 8. Having set the stop condition parameter  $C$  to 5 for these examples, the Breadth-First Search continues until the auxiliary queue achieves the state 07 in the first case, and state 19 in the second case, when precisely  $\Sigma$  equals  $C$ , since the auxiliary queue has been continuously run through for 5 times. The stop condition parameter  $C$  has been empirically defined by taking into account a sufficient distance far away from the critical region to compute the outwards direction vectors.

Thus, the leftover pixels in the auxiliary queue, say **i** and **j** in the first case, and **u**, **v** and **x** in the second case, are precisely the end points of the required outwards direction vectors  $\vec{v}_i$ , obviously non-normalized yet. Besides the end points, the origin points are also needed to compute each outward segment direction vector. In order to find the origin points, every candidate should satisfy two requisites at the same time: (i) being the closest neighbor to a critical region pixel and (ii) having a path of valid pixels between it and the corresponding end point. For skeletons with low densities of critical regions, one may relax these requirements to only the first condition. However, in some cases the latter requisite is mandatory so as

Table A.2

Breadth First Search across a bifurcation of type 4: auxiliary queue states.  $B$  is set to 1 whenever every pixel in a specific state is non-critical and 0 otherwise.  $\Sigma$  increases by one if the respective  $B$  variable has been set to 1, and zeroed otherwise. Already dequeued pixels have been concealed.

state	current	auxiliary queue	B	$\Sigma$
00	a	b	0	0
01	b	c d	0	0
02	c	d e	0	0
03	d	e f	1	1
04	e	f g	1	2
05	f	g h	1	3
06	g	h i	1	4
07	h	i j	0	0
08	i	j k	0	0
09	j	k l m	0	0
10	k	l m n	0	0
11	l	m n o p	0	0
12	m	n o p	0	0
13	n	o p q	0	0
14	o	p q r	0	0
15	p	q r s	1	1
16	q	r s t	1	2
17	r	s t u	1	3
18	s	t u v	1	4
19	t	u v x	1	5

to correctly find out each origin point direction vector, since it may happen that there is a closest neighbor to a critical region which does not pertain to the current branch. In the cases illustrated in Fig. 1(a) and Fig. 1(b), it is sufficient to take into account only condition (i). Afterwards, each outwards direction vector is normalized and inner products between the unitary inwards direction vector  $\hat{v}_0$  and each unitary outwards direction vector are computed. As a consequence, the unitary outwards direction vector for which the inner product attains its maximum result, in accordance with Eq. 1, gives the optimum direction to continue the tracking with the very same label value, hence providing the following pixel to be stacked. The remaining vectors origins are enqueued as secondary seeds. Both examples show non-normalized outward direction vectors, being  $\vec{v}_1$  the optimum direction choice to continue the tracking beyond the critical region, whereas the remaining vectors  $\vec{v}_i$  are shown as side branches directions to be considered later on.

## A.2 Critical Regions Classification Rules

Let  $S$  be a set of critical regions  $S = \{s_1, s_2, s_3 \dots\}$ ,  $s_1$  being the current critical region and  $D_{max}$  the shortest allowed path length between two consecutive critical regions. Let  $\hat{v}_0$  be the unitary **inwards** vector to  $s_1$  and let  $E_1$  and  $E_2$  be the sets of unitary **outwards** vectors from close critical regions  $s_1$  and  $s_2$  respectively. Let  $|E_i|$  be the cardinality of  $E_i$ . Then, a critical region should be classified into one of the eight classes depicted in the Fig. 9, according to the following rules:

- (1) **Bifurcation 1:** Fig. 4(a)  
 $|E_1| = 2$  and  
 $\langle \hat{v}_0, \hat{v}_i \rangle > 0, \quad \forall \hat{v}_i \in E_1$
- (2) **Bifurcation 2:** Fig. 4(b)  
 $|E_1| = 2$  and  
 $\exists \hat{v}_i, \hat{v}_j \in E_1 \mid$   
 $\langle \hat{v}_0, \hat{v}_i \rangle > 0$  and  $\langle \hat{v}_0, \hat{v}_j \rangle \leq 0$  and  
 $\nexists s_2 \mid dist(s_1, s_2) < D_{max}$
- (3) **Bifurcation 3:** Fig. 4(c)  
 $|E_1| = 2$ , but  
 $\exists s_2 \mid dist(s_1, s_2) < D_{max} \therefore |E_1| + |E_2| = 3$   
 $\exists \hat{v}_j \in s_1$  e  $\hat{v}_k, \hat{v}_l \in s_2$ , such that  
 $\langle \hat{v}_0, \hat{v}_k \rangle \approx 1$  and  $\langle \hat{v}_j, \hat{v}_l \rangle \neq -1$
- (4) **Bifurcation 4:** Fig. 4(d)  
 $|E_1| = 2$ , but  
 $\exists s_2 \mid dist(s_1, s_2) < D_{max} \therefore |E_1| + |E_2| = 3$   
 $\exists \hat{v}_j \in s_1$  e  $\hat{v}_k, \hat{v}_l \in s_2$ , such that  
 $\langle \hat{v}_0, \hat{v}_k \rangle \approx 1$  ,  $\langle \hat{v}_j, \hat{v}_l \rangle \neq -1$   
and  $\langle \hat{v}_0, \hat{v}_j \rangle \leq 0$
- (5) **Superposition:** Fig. 4(e)  
 $|E_1| = 2$ , but  
 $\exists s_2 \mid dist(s_1, s_2) < D_{max} \therefore |E_1| + |E_2| = 3$   
 $\exists \hat{v}_j \in s_1$  and  $\hat{v}_k, \hat{v}_l \in s_2$ , such that  
 $\langle \hat{v}_0, \hat{v}_j \rangle \leq 0$ , and  
 $\langle \hat{v}_0, \hat{v}_k \rangle \approx 1$  and  $\langle \hat{v}_j, \hat{v}_l \rangle \approx -1$
- (6) **Crossing:** Fig. 4(f)  
 $|E_1| = 3$  and  
 $\exists \hat{v}_j, \hat{v}_k, \hat{v}_l \in s_1$  such that  
 $\langle \hat{v}_0, \hat{v}_k \rangle \approx 1$  and  $\langle \hat{v}_j, \hat{v}_l \rangle \approx -1$

## Acknowledgement

The authors are grateful to Fapesp, CNPq, Capes and Finep for financial support, as well as to the *Nature Publishing Group* for the license to use the images in [18].

## References

- [1] S. Arulampalam, S. Maskell, N. Gordon, T. Clapp, A tutorial on particle filters for on-line non-linear/non-gaussian bayesian tracking, *IEEE Transactions on Signal Processing* 50 (2) (2002) 174–188.
- [2] J. Bresenham, Algorithm for computer control of a digital plotter, *IBM Systems Journal* 4 (1) (1965) 25–30.
- [3] F. Caserta, H. Stanley, W. Eldred, G. Daccord, R. Haussman, J. Nittmann, Physical mechanisms underlying neurite outgrowth: A quantitative analysis of neuronal shape, *Physical Review Letters* 64 (1) (1990) 95–98.
- [4] K. R. Castleman, *Digital Image Processing*, Prentice-Hall, Englewood Cliffs, NJ, 1979.
- [5] R. M. Cesar-Jr., L. da F. Costa, Neural cell classification using wavelets and multiscale curvature, *Biological Cybernetics* 79 (4) (1998) 347–360.
- [6] R. M. Cesar-Jr., L. da F. Costa, Dendrogram generation for neural shape analysis, *The Journal of Neuroscience Methods* 93 (1999) 121–131.
- [7] L. da F. Costa, Morphological complex networks: Can individual morphology determine the general connectivity and dynamics of networks?, in: COSIN 2005 Final meeting, Conference on Complex Networks, Salou, Spain, 2005, <http://xxx.lanl.gov/abs/q-bio.MN/0503041>.
- [8] L. da F. Costa, R. M. Cesar-Jr., *Shape Analysis and Classification: Theory and Practice*, CRC Press, 2001.
- [9] L. da F. Costa, E. Manoel, F. Faucereau, J. Chelly, J. van Pelt, G. Ramakers, A shape analysis framework for neuromorphometry, *Network: Computation in Neural Systems* 13 (August 2002) 283–310(28), <http://www.ingentaconnect.com/content/apl/network/2002/00000013/00000003/art00303>.
- [10] E. R. Dougherty, R. A. Lotufo, *Hands-On Morphological Image Processing*, SPIE-International Society for Optical Engine, 2003.
- [11] P. F. Gabriel, J. G. Verly, J. H. Piater, A. Genon, The state of the art in multiple object tracking under occlusion in video sequences, in: *In Advanced Concepts for Intelligent Vision Systems (ACIVS)*, 2003, 2003.
- [12] G. T. Herman, *Geometry of Digital Spaces*, Birkhauser Boston, 1998.



- [13] S. Information Systems, SDC Morphology Toolbox for Matlab, <http://www.mmorph.com/>, version 1.5 (October 2006).
- [14] H. Jelinek, E. Fernandez, Neurons and fractals: How reliable and useful are calculations of fractal dimensions?, *Journal of Neuroscience Methods* 81 (1-2) (1998) 9–18.
- [15] J. J. G. Leandro, R. M. Cesar-Jr., L. da F. Costa, Determining the branching structure of 3D structures from respective 2D projections, in: *Proc. 19th SIBGRAPI - Brazilian Symposium on Computer Graphics and Image Processing*, IEEE Computer Society Press, 2006.
- [16] J. J. G. Leandro, R. M. Cesar Jr, L. da F. Costa, Automatic contour extraction from 2d neuron images, <http://aps.arxiv.org/abs/0804.3234> (2008).
- [17] J. J. G. Leandro, R. M. Cesar-Jr., L. da F. Costa, Automatic contour extraction of neurons in presence of overlap, in: *Workshop on Bio-Image Informatics: Biological Imaging, Computer Vision and Data Mining, 2008*, Santa Barbara, CA, USA, 2008, <http://www.ece.ucsb.edu/bioimage/workshop2008/index.html>.
- [18] R. H. Masland, The fundamental plan of the retina, *Nature Neuroscience* 4 (9) (2001) 877–886.
- [19] K. Morigiwa, M. Tauci, Y. Fukuda, Fractal analysis of ganglion cell dendritic branching patterns of the rat and cat retinae, *Neuroscience Research Suppl.* 10 (1989) S131–S140.
- [20] M. B. L. Rocchi, D. Sisti, M. C. Albertini, L. Teodori, Current trends in shape and texture analysis in neurology: Aspects of the morphological substrate of volume and wiring transmission, *Brain Research Reviews* 55 (2007) 97–107.
- [21] K. Rothaus, P. Rhiem, X. Jiang, Separation of the retinal vascular graph in arteries and veins, in: F. Escolano, M. Vento (eds.), *GbRPR 2007, Graph-Based Representations in Pattern Recognition, 6th IAPR-TC-15 International Workshop*, Alicante, Spain, Proceedings, vol. 4538 of *Lecture Notes in Computer Science*, Springer Verlag, 2007, <http://www.springerlink.com/content/d573048432h4k13x/>.
- [22] K. Rothaus, P. Rhiem, X. Jiang, Separation of the retinal vascular graph based upon structural knowledge, doi:10.1016/j.imavis.2008.02.013, in press, *Image and Vision Computing* (2008).
- [23] R. Sedgewick, *Algorithms*, Addison-Wesley Publishing Company, Reading, MA, USA, 1983.
- [24] P. Soille, *Morphological Image Analysis: Principles and Applications*, Springer Verlag, 1999.

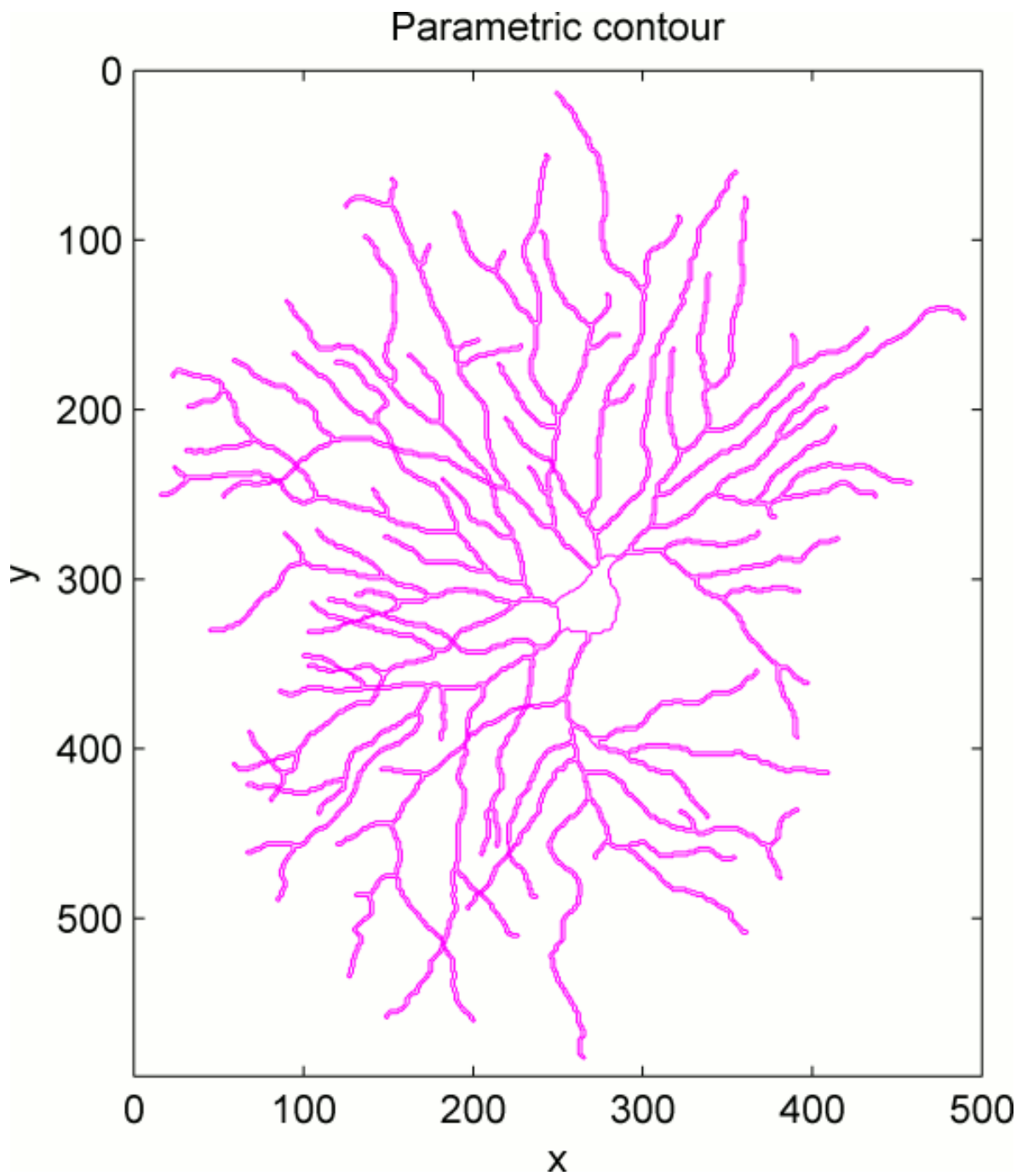


Fig. 15. Parametric contour resulting from the *BSCEA* application on a neuron *Alfa* image. Notice how the *BSCEA* grants full admittance to all the innermost regions within the neuron image. Also, note the contour continuity across critical regions.

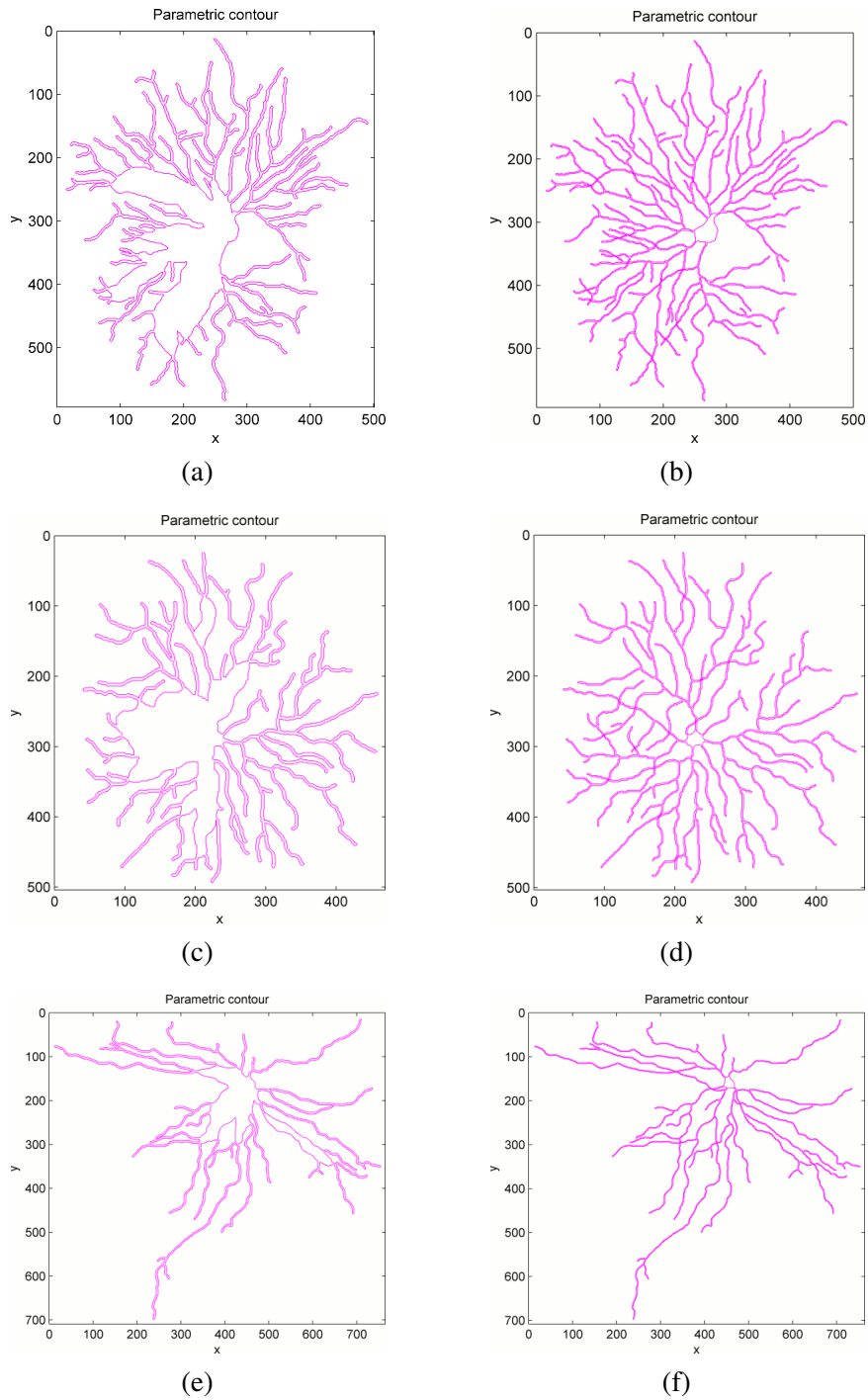


Fig. 16. Comparison for alpha, delta and epsilon neuron images between results yielded by the traditional (a-c-e) and (b-d-f) BSCEA algorithms. The *BSCEA* enters all the regions, surpassing the traditional algorithm.

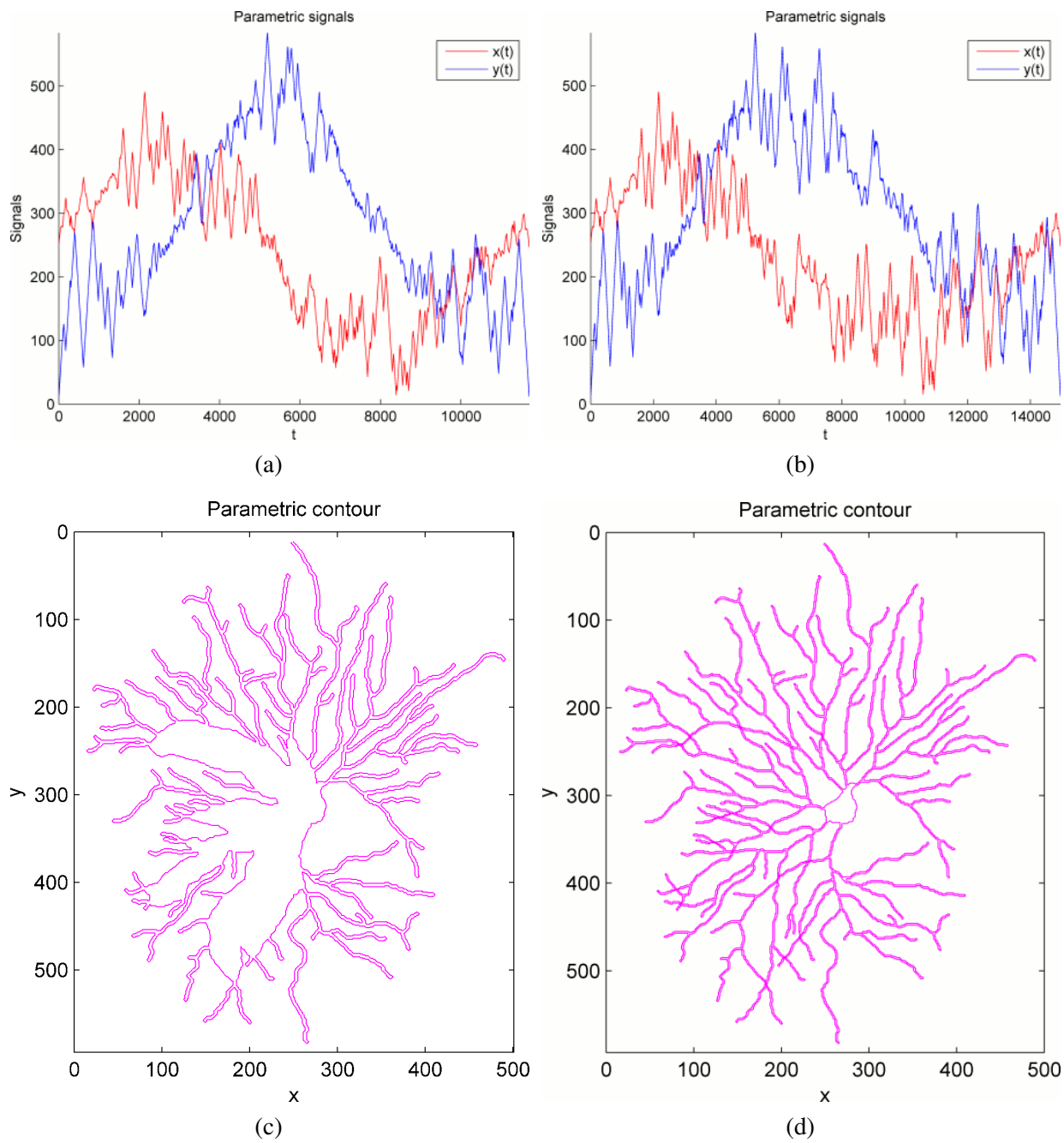


Fig. 17. Comparison for an *alpha* neuron image between results yielded by the algorithms (a-c) Traditional and (b-d) BSCEA. The *BSCEA* enters all the regions, surpassing the traditional algorithm in over than two thousand contour points.

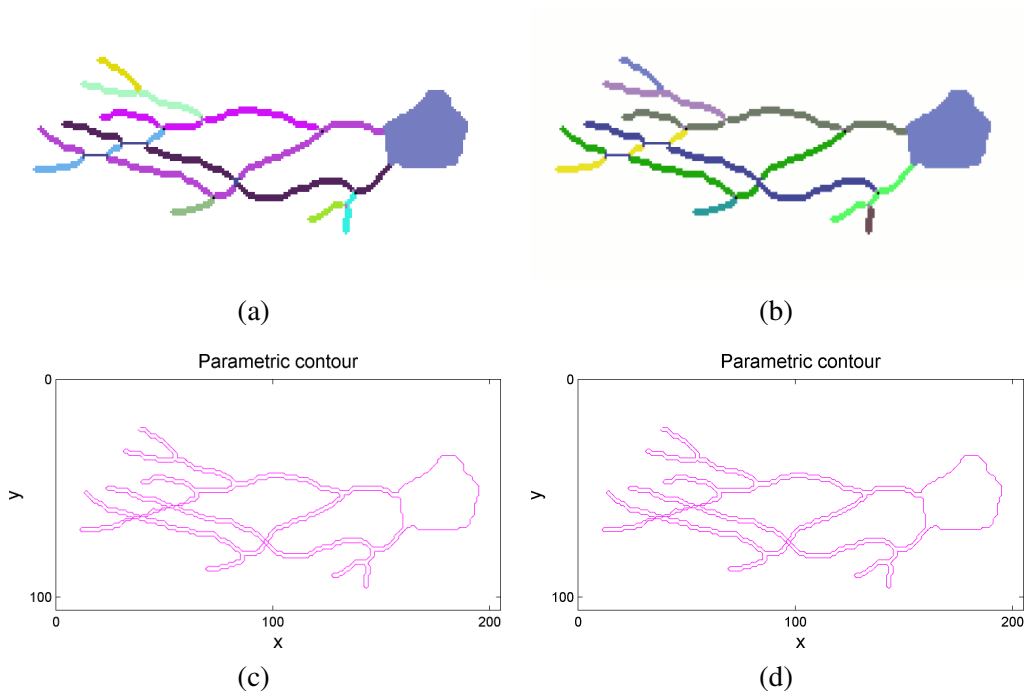


Fig. 18. Comparison between a synthetic neuron shape labeled automatically (a) and manually (b). Parametric contours provided by the BSCEA for the automatic (c) and manual (d) labelings. Despite minor differences between automatic and manual labelings, notice that both contours are in complete accordance.

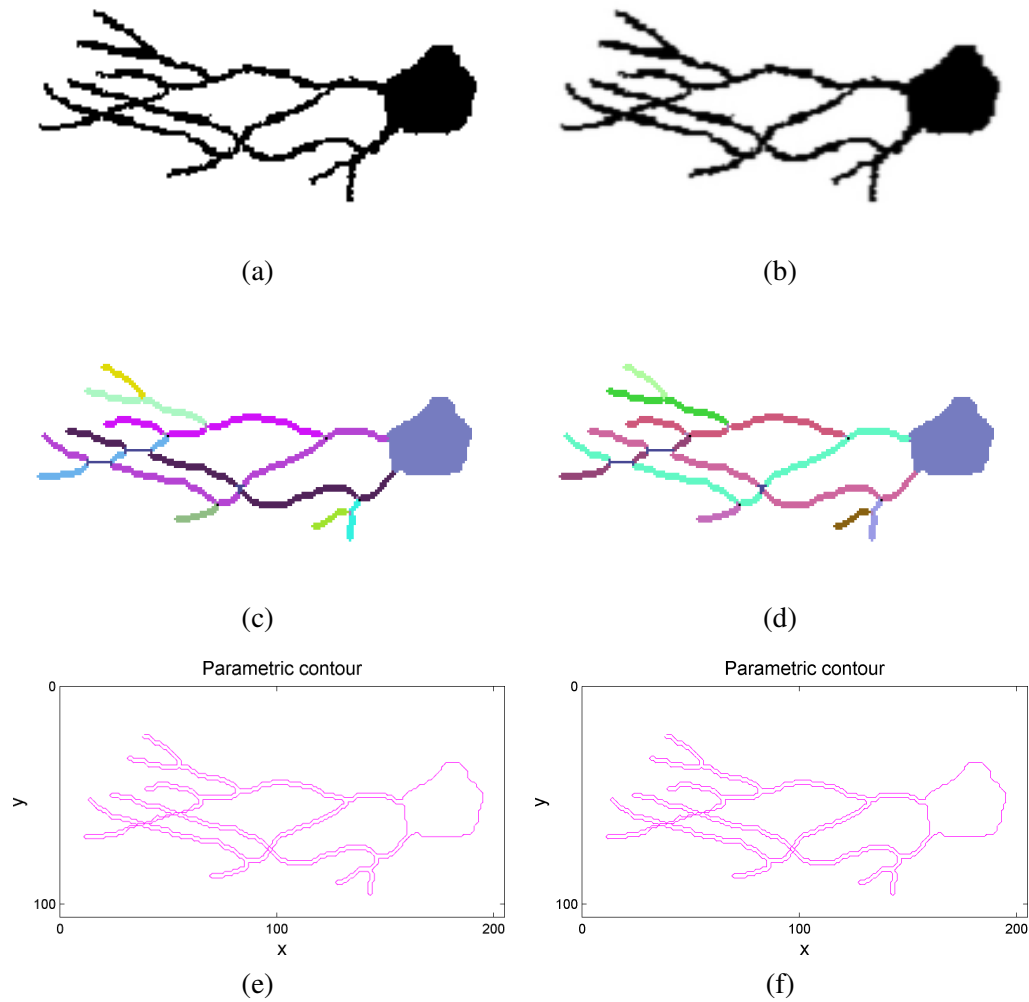


Fig. 19. Assessment of noise effects on neuron shape labeling and respective contour extraction. A synthetic neuron shape has been corrupted by  $2D$  Gaussians with different bandwidths. The Gaussian scale parameters  $\sigma$  in Fourier domain varied from  $10^{-8}$  up to  $2 \cdot 10^{-6}$ . Both BTA and BSCEA ensured robustness within this range of smoothing bandwidths.

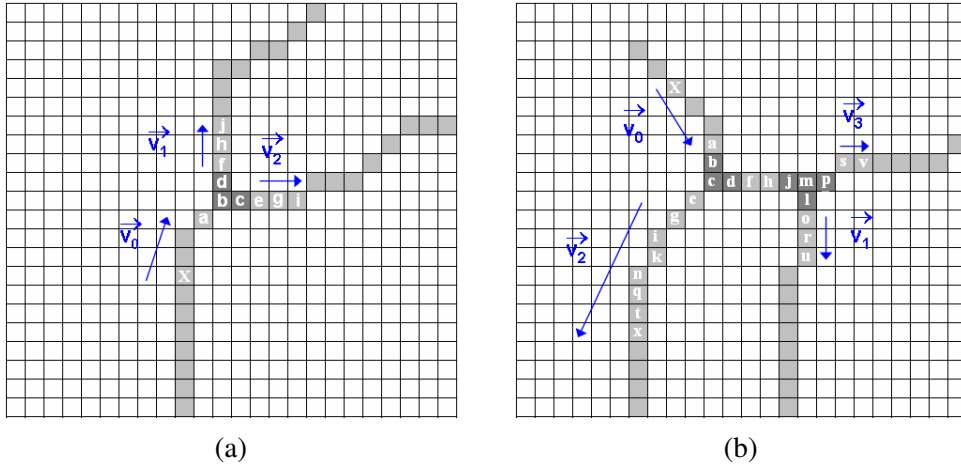


Fig. A.1. *Breadth First Search* application to find out extremity points for outwards direction vectors calculation. The **X**-marked pixel address is provided by the *backpointer* as the origin of the inwards direction vector  $\vec{v}_0$ . Pixels appear in alphabetical order portraying the Breadth First Search visitation order, according to the chain-code scanning. (a) A bifurcation 1 and its direction vectors. The Breadth-First Search starts up when the pixel *b* is detected and ceases when there remain solely the pixels *i* and *j* in the auxiliary queue. (b) A bifurcation 4 and its direction vectors. When two critical regions of type bifurcation 1 occur highly close to each other, the agglutination effect takes place and two bifurcations 1 are seen as a bifurcation 4. The Breadth-First Search starts up when the pixel *b* is detected and ceases when there remain solely the pixels *u*, *v* and *x* in the auxiliary queue.

3	2	1
4	C	8
5	6	7

Fig. A.2. Neighborhood defined by the chain-code and used by the *BTA* and *BSCEA*

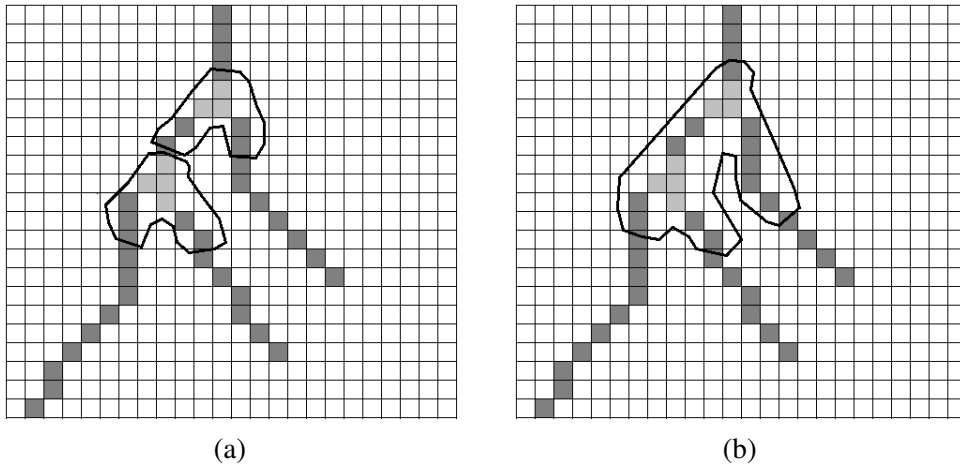


Fig. A.3. (a) Two distinct bifurcations of type 1 will be seen as (b) one bifurcation of type 4, an immediate consequence from the *agglutinating effect* caused by the Breadth First Search algorithm, when encountering two close bifurcations, as though the current local analysis had given place to a more global analysis by switching into a larger analyzing scale